

Efficient Implementation of Finite Element Methods for Spatial Fractional PDEs in Three Dimensions

Zongze Yang^a, Zhanbin Yuan^a, Yufeng Nie^a, Jungang Wang^{a,*}

^aDepartment of Applied Mathematics, Northwestern Polytechnical University, Xi'an, Shaanxi 710072, China

Abstract

In this paper, we address the main challenges of the implementation of finite element methods for solving spatial fractional problems on three dimensional irregular convex regions. Different from the integer case, the non-locality of fractional derivative operators makes the assembly of fractional stiffness matrix much more difficult, mainly in two aspects: one is the search of the integral path of Gaussian points, and the other is the calculation of fractional derivatives of basis functions at Gaussian points. By introducing the ray-simplex intersection algorithm, we present an efficient method for finding integration paths of Gaussian points. By analyzing the expression of the fractional derivative of finite element basis functions, we give a method for efficiently calculating the fractional derivative. In order to speed up the procedure in MATLAB, some implementation techniques are introduced. We demonstrate our method by applying it to different problems, including steady and transient spatial fractional problems.

Keywords: finite element method, fractional derivatives, three dimensions, irregular domains, algorithm, implementation

1. Introduction

Fractional calculus has become increasingly used as a modeling tool in numerous diverse fields, such as physics[37, 48], finance[23, 40] and hydrology[4, 49]. The main reason behind this is its suitability for explaining non-local and memory phenomena in complex systems in these fields. However, due to these anomalous properties, it is difficult to get close form solutions of fractional partial differential equations (FPDEs). Thus, a number of numerical methods have been developed, such as finite element methods, finite difference methods, spectral methods and etc.

Finite element method(FEM), a widely used method in engineering, has been generalized to solve FPDEs by many researchers. After Ervin and Roop developed the theoretical framework for FEM[16, 38], many aspects of FEM have been studied, such as existence, uniqueness and regularity of weak solution to fractional problems[25, 26, 42, 44]. Deng [14] developed FEM for the space and time fractional FokkerPlanck equation and established stability and error estimates rigorously. In [47], Zhang et al. solved symmetric space-fractional partial differential equations with homogeneous boundary condition, and they analyzed the existence of the variational solution as well as the stability and convergence of the discrete scheme they developed. Zheng et al.[55] considered FEM for the space-fractional advection diffusion equation of Caputo fractional operator with non-homogeneous boundary condition dealt by classical technical. Zhao and Li[53] developed finite difference/element approximations for the timespace fractional telegraph equation. The variational form of their scheme is non-symmetric because they used a non-symmetric decomposition of the fractional order of derivative operator. They proved the existence and the uniqueness of the weak solution, and discussed the stability and convergence of their numerical schemes. In another paper[54], they solved a generalized nonlinear fractional FokkerPlanck equation by fully discrete Galerkin FEM. In [56], Zhuang et al. proposed a one-dimensional space-fractional Boussinesq equation and developed finite volume and finite element methods for the equation, respectively. Xu and Hesthaven[45] proposed a discontinuous Galerkin

*Corresponding author

Email address: wangjungang@nwpu.edu.cn (Jungang Wang)

method for fractional convection-diffusion equations by decomposed the equation into a low order system. The stability and optimal order of convergence is proved in their paper. In [43], the authors investigated finite element approximation for inhomogeneous Dirichlet boundary-value problems of space-fractional diffusion equations with Caputo operator. Guan and Gunzburger[24] developed FEM for fractional diffusion equations with localized generalization of the fractional Laplacian operator, which is similar with peridynamics model. In [28], Jin and Zhou proposed a singularity reconstruction strategy, where the solution is split into a singular part and a regular part, to improve the convergence order of finite element for fractional boundary value problems. In addition, they established error estimates for the Galerkin approximation rigorously. And then, in paper [27], Jin et al. discussed Petrov-Galerkin FEM for fractional boundary value problems with Riemann-Liouville and Caputo derivative of order $\alpha \in (3/2, 2)$. In [21], Feng et al. developed finite element method for space-time fractional diffusion equation. Li and his coworkers investigated finite element for nonlinear FDEs, including nonlinear fractional Schrödinger equations and nonlinear fractional Ginzburg-Landau equation in a series of publications[31–35]. Çelik and Duman [11] considered FEM for fractional diffusion equation involving symmetric tempered fractional derivative operators and carried out the stability and error estimates of the numerical scheme. Zhao et al.[51] developed adaptive finite element method for fractional differential equations using hierarchical matrices by combining adaptive algorithms with geometric multigrid method based on hierarchical matrices. Li and Wang et al.[36] established fast finite element algorithms for variable-coefficient fractional diffusion equations. And Zhao et al.[50] presented a fast Hermite FEM for space-fractional diffusion equation by exploiting properties of the stiffness matrix on uniform mesh.

There are so many works on FEM for FPDEs, but the papers cited above almost all focus on one dimensional(1-D) spatial fractional differential equations. Many researchers have investigated spatial FPDE with Riemann-Liouville fractional operator on two dimensional(2-D) domains. In [39], Roop considered FEM for fractional advection dispersion equation on 2-D bounded domains. Bu et al.[8] developed Galerkin FEM for 2-D Riesz spatial FPDEs with detailed theoretical analysis. Later, they proposed Crank-Nicolson ADI Galerkin FEM for the same equation[6], and applied the method to solve fractional FitzHugh-Nagumo monodomain model arising from electro-physiology[9]. Also, Bu applied FEM to solve space and time fractional Bloch-Torrey equations[7]. Zhao et al.[52] discussed Crank-Nicolson Galerkin fully-discrete schemes for 2-D spatial fractional advection-dispersion equations with only left Riemann-Liouville fractional operator. Du and Wang[15] developed fast finite element method for space-fractional dispersion equations on 2-D uniform meshes. Most of these works studied finite element methods on 2-D domains using uniform structured meshes. In [46], Yang et al. developed FEM for nonlinear Riesz space fractional diffusion equations using unstructured meshes. Fan et al.[18–20] considered FEM for solving the time-space fractional wave equation and time-space fractional Schrödinger equation using unstructured meshes on 2-D domain. Dehghan and Abbaszadeh [12, 13] solved two-dimensional space-multi-time fractional Bloch-Torrey equations using FEM, and proposed finite difference/finite element to solve one- and two-dimensional space fractional tempered fractional diffusion-wave equations.

As we know, for fractional derivatives, especially for fractional Laplacian, there are many different definitions, which are proved to be equivalent for sufficiently smooth functions in \mathbb{R}^n [30]. However this equivalence no longer holds for functions on bounded domains. Except for FPDEs with fractional Laplacian defined by Riesz fractional operator, researchers have developed FEM for FPDEs with integral definition of fractional Laplacian. Acosta and his coworkers[1, 2] presented a complete n -dimensional finite element analysis of the homogeneous Dirichlet problem associated to fractional Laplacian by integral definition and gave a finite element implementation for a 2-D homogeneous Dirichlet problem. Borthagaray et al.[5] investigated FEM for finding solutions to the eigenvalue problem for the fractional Laplacian, and the numerical experiments were presented in 1-D and 2-D domains. To avoid dealing with fractional operator, Ainsworth and Glusa [3] proposed hybrid finite element-spectral method for the fractional Laplacian based on extension problem presented by Caffarelli and Silvestre [10].

Though there are so many works on FEM for spatial FPDEs, most of them focus on one or two dimensional problems. Spatial FPDEs on three dimensional(3-D) domains are seldom solved in literatures. The main focus of this work is on FEM to solve 3-D spatial FPDEs with Riemann-Liouville fractional derivatives and Riesz fractional derivatives.

Steady and transient fractional problems always have following form

$$\begin{aligned} Lu(\mathbf{x}) &= f(\mathbf{x}), \quad \mathbf{x} \in \Omega, \\ u_t(\mathbf{x}) + Lu(\mathbf{x}) &= f(\mathbf{x}), \quad \mathbf{x} \in \Omega, \end{aligned} \tag{1}$$

where L is a linear operator consisting of fractional operators defined in section 2 and Ω is an open convex set in \mathbb{R}^n ($n = 1, 2, 3$). In applications, $Lu(\mathbf{x})$ mainly contains three forms listed below.

- Case 1: $c(\mathbf{x})\mathcal{D}_i^{2\alpha}u(\mathbf{x})$ or written as $c(\mathbf{x})\mathcal{D}_i^{1+\beta}u(\mathbf{x})$,
- Case 2: $\mathcal{D}_i(c(\mathbf{x})\mathcal{D}_i^\beta u(\mathbf{x}))$,
- Case 3: $\mathcal{D}_i^\beta(c(\mathbf{x})\mathcal{D}_i u(\mathbf{x}))$,

where $1/2 < \alpha < 1$, $0 < \beta < 1$, and \mathcal{D}_i^μ ($\mu > 0$) is left or right Riemann-Liouville fractional derivative operator with respect to x_i , and \mathcal{D}_i is an abbreviate of classical first order derivative operator $\frac{\partial}{\partial x_i}$. When $c_i(\mathbf{x})$ is constant and $u(\mathbf{x})$ is zero on the boundary, these three forms are equivalent mathematically. In addition, denote operator $\mathcal{D}_i^{\mu*}$ as the adjoint form of \mathcal{D}_i^μ , i.e., if \mathcal{D}_i^μ is left Riemann-Liouville fractional derivative operator, then $\mathcal{D}_i^{\mu*}$ is right Riemann-Liouville fractional derivative operator of the same order. By this symbol, it is easy to see that $\mathcal{D}_i^{1*} = -\mathcal{D}_i^1$. Note that the notation \mathcal{D}_i^1 is different with \mathcal{D}_i . The former represents left or right Riemann-Liouville fractional derivative operator while the latter represents classical first order derivative operator. By calculation, the variational forms of those three cases have a uniform form (see section 2.2)

$$(c(\mathbf{x})\mathcal{D}_i^\alpha u(\mathbf{x}), \mathcal{D}_i^{\beta*} v(\mathbf{x})) \tag{2}$$

where $0 \leq \alpha, \beta \leq 1$.

In this paper, we mainly discuss how to handle form (2), i.e. how to assemble stiffness matrix for this form. From form (2), we notice that assembling stiffness matrix is related with the calculation of fractional derivatives of basis functions and this is much more complicated than the calculation of integer derivatives. Computation of fractional derivatives depends on the paths of integration starting with the Gaussian points. This is the main challenge in the implementation of FEM for spatial fractional PDEs. In the literatures, researchers have introduced some ways to search the paths with very tedious procedures. The integration paths are made of intersection segments of the rays starting with Gaussian points along certain direction with elements. If we use simplex elements (this is always the case), we can easily compute the intersection segments by using the algorithm presented below, named as the ray-simplex intersection algorithm. And we can simplify the procedure of computing fractional derivatives by the algorithm.

This paper is arranged as follows: section 2 is devoted to describe some notations involved. Algorithms on assembling fractional stiffness matrix for the variational form is discussed in section 3 including assembling element fractional stiffness matrix, finding integral path for Gaussian points and some details on implementation with MATLAB. In section 4, we apply the algorithms to solve 3-D steady/transient fractional problems. And conclusions are given in the last section.

2. Preliminary

In this section, we will introduce some norms and spaces involved with fractional calculus and deduce variational forms for different type terms in L . In the following sections, we denote (\cdot, \cdot) as inner product in $L^2(\Omega)$.

2.1. Notations

Let $\mathbf{x} = (x_1, \dots, x_n)^T$, $\mathbf{y} = (y_1, \dots, y_n)^T$ be points in \mathbb{R}^n . Define \mathbf{e}_i ($i = 1, 2, \dots, n$) the unit column vector, of which the i^{th} component is 1. Unless otherwise specified, we do not distinguish points from column vectors in following sections. Based on the notations defined above, we can characterize the boundary of convex domain Ω by $a_i(\mathbf{x})$ and $b_i(\mathbf{x})$ as below,

$$\begin{aligned} a_i(\mathbf{x}) &:= \inf\{y_i | \mathbf{y} = \mathbf{x} + k\mathbf{e}_i, \mathbf{y} \in \Omega, k \in \mathbb{R}\}, \\ b_i(\mathbf{x}) &:= \sup\{y_i | \mathbf{y} = \mathbf{x} + k\mathbf{e}_i, \mathbf{y} \in \Omega, k \in \mathbb{R}\}. \end{aligned} \tag{3}$$

Here, $a_i(\mathbf{x})$ and $b_i(\mathbf{x})$ respectively represent the lower and upper bounds of the line segment parallel to \mathbf{e}_i through point \mathbf{x} .

Then, some definitions of fractional calculus are listed, including Riemann-Liouville fractional integral operator, Riemann-Liouville fractional derivative operator and Riesz fractional derivative operator.

Definition 1. Let $\alpha > 0$, $f(\mathbf{x}) \in L_1(\Omega)$. Then the Riemann-Liouville fractional integral operators ${}_{a_i(\mathbf{x})}I_{x_i}^\alpha$ and ${}_{x_i}I_{b_i(\mathbf{x})}^\alpha$ of order $\alpha > 0$ are defined by

$${}_{a_i(\mathbf{x})}I_{x_i}^\alpha f(\mathbf{x}) := \frac{1}{\Gamma(\alpha)} \int_{a_i(\mathbf{x})}^{x_i} (x_i - y_i)^{\alpha-1} f(\mathbf{x} + (y_i - x_i)\mathbf{e}_i) dy_i, \quad (4)$$

$${}_{x_i}I_{b_i(\mathbf{x})}^\alpha f(\mathbf{x}) := \frac{1}{\Gamma(\alpha)} \int_{x_i}^{b_i(\mathbf{x})} (y_i - x_i)^{\alpha-1} f(\mathbf{x} + (y_i - x_i)\mathbf{e}_i) dy_i. \quad (5)$$

Definition 2. Let $m - 1 < \alpha < m$, $m \in \mathbb{N}_+$, $f(\mathbf{x})$ defined on Ω . Then the Riemann-Liouville fractional derivative operators ${}_{a_i(\mathbf{x})}^{\text{RL}}\mathcal{D}_{x_i}^\alpha$ and ${}_{x_i}^{\text{RL}}\mathcal{D}_{b_i(\mathbf{x})}^\alpha$ of order α are defined by

$$\begin{aligned} {}_{a_i(\mathbf{x})}^{\text{RL}}\mathcal{D}_{x_i}^\alpha f(\mathbf{x}) &:= \frac{d^m}{dx_i^m} {}_{a_i(\mathbf{x})}I_{x_i}^{m-\alpha} f(\mathbf{x}), \\ {}_{x_i}^{\text{RL}}\mathcal{D}_{b_i(\mathbf{x})}^\alpha f(\mathbf{x}) &:= (-1)^m \frac{d^m}{dx_i^m} {}_{x_i}I_{b_i(\mathbf{x})}^{m-\alpha} f(\mathbf{x}). \end{aligned} \quad (6)$$

Definition 3. Let $\alpha > 0$, $f(\mathbf{x})$ defined on Ω . Then the Riesz fractional derivative ${}^{\text{Rz}}\mathcal{D}_{x_i}^\alpha f(\mathbf{x})$ of order $\alpha > 0$ is defined by

$${}^{\text{Rz}}\mathcal{D}_{x_i}^{2\alpha} f(\mathbf{x}) := -c_\alpha \left({}_{a_i(\mathbf{x})}^{\text{RL}}\mathcal{D}_{x_i}^{2\alpha} f(\mathbf{x}) + {}_{x_i}^{\text{RL}}\mathcal{D}_{b_i(\mathbf{x})}^{2\alpha} f(\mathbf{x}) \right), \quad (7)$$

where $c_\alpha = \frac{1}{2 \cos(\pi\alpha)}$.

From the definition of Riesz fractional derivative, we know that when $\alpha = 2$ it is same with the classical derivative of order 2.

Next, let us borrow some notations on fractional Sobolev spaces from Ervin and Roop[16, 17].

Definition 4. Let $\mu > 0$. Define the semi-norm

$$|u|_{J_L^\mu(\Omega)} := \left(\sum_{i=1}^n \| {}_{a_i(\mathbf{x})}^{\text{RL}}\mathcal{D}_{x_i}^\mu u \|_{L^2(\Omega)}^2 \right)^{1/2}$$

and the norm

$$\|u\|_{J_L^\mu(\Omega)} := \left(\|u\|_{L^2(\Omega)}^2 + |u|_{J_L^\mu(\Omega)}^2 \right)^{1/2}.$$

And denote $J_L^\mu(\Omega)$ ($J_{L,0}^\mu(\Omega)$) as the closure of $C^\infty(\Omega)$ ($C_0^\infty(\Omega)$) with respect to $\|\cdot\|_{J_L^\mu(\Omega)}$.

Definition 5. Let $\mu > 0$. Define the semi-norm

$$|u|_{J_R^\mu(\Omega)} := \left(\sum_{i=1}^n \| {}_{x_i}^{\text{RL}}\mathcal{D}_{b_i(\mathbf{x})}^\mu u \|_{L^2(\Omega)}^2 \right)^{1/2}$$

and the norm

$$\|u\|_{J_R^\mu(\Omega)} = \left(\|u\|_{L^2(\Omega)}^2 + |u|_{J_R^\mu(\Omega)}^2 \right)^{1/2}.$$

And denote $J_R^\mu(\Omega)$ ($J_{R,0}^\mu(\Omega)$) as the closure of $C^\infty(\Omega)$ ($C_0^\infty(\Omega)$) with respect to $\|\cdot\|_{J_R^\mu(\Omega)}$.

Definition 6. Let $\mu \neq m - 1/2$, $m \in \mathbb{N}$. Define the semi-norm

$$|u|_{J_S^\mu(\Omega)} = \left(\sum_{i=1}^n \left| ({}_{a_i(\mathbf{x})}^{\text{RL}}\mathcal{D}_{x_i}^\mu u, {}_{x_i}^{\text{RL}}\mathcal{D}_{b_i(\mathbf{x})}^\mu u) \right| \right)^{1/2}$$

and the norm

$$\|u\|_{J_S^\mu(\Omega)} = \left(\|u\|_{L^2(\Omega)}^2 + |u|_{J_S^\mu(\Omega)}^2 \right)^{1/2}.$$

And denote $J_S^\mu(\Omega)$ ($J_{S,0}^\mu(\Omega)$) as the closure of $C^\infty(\Omega)$ ($C_0^\infty(\Omega)$) with respect to $\|\cdot\|_{J_S^\mu(\Omega)}$.

Definition 7. Let $\mu > 0$. Define the semi-norm

$$|u|_{H^\mu(\Omega)} = \|\omega|^\mu \mathcal{F}(\hat{u})(\omega)\|_{L^2(\mathbb{R}^n)}$$

and the norm

$$\|u\|_{H^\mu(\Omega)} = (\|u\|_{L^2(\Omega)}^2 + |u|_{H^\mu(\Omega)}^2)^{1/2}$$

where $\mathcal{F}(\hat{u})(\omega)$ is the Fourier transformation of function \hat{u} , \hat{u} is the zero extension of u outside Ω , and denote $H^\mu(\Omega)$ ($H_0^\mu(\Omega)$) as the closure of $C^\infty(\Omega)$ ($C_0^\infty(\Omega)$) with respect to $\|\cdot\|_{H^\mu(\Omega)}$.

The following lemma states that the spaces $J_{L,0}^\mu(\Omega)$, $J_{R,0}^\mu(\Omega)$, $J_{S,0}^\mu(\Omega)$ and $H_0^\mu(\Omega)$ are equivalent with equivalent semi-norms and norms if $\mu \neq m - 1/2$ ($m \in \mathbb{N}$). All proofs are omitted for they are similar with 2-D cases which have been proved in literatures[17, 38, 46, 47].

Lemma 2.1 ([17]). *Let $\mu \neq m - 1/2$ ($m \in \mathbb{N}$), and $u \in J_{L,0}^\mu(\Omega) \cap J_{R,0}^\mu(\Omega) \cap H_0^\mu(\Omega)$. Then there exist positive constants C_1 and C_2 independent of u such that*

$$C_1 |u|_{H^\mu(\Omega)} \leq \max\{|u|_{J_L^\mu(\Omega)}, |u|_{J_R^\mu(\Omega)}\} \leq C_2 |u|_{H^\mu(\Omega)}. \quad (8)$$

Lemma 2.2 ([17]). *Let $\mu > 0$, $u \in J_{L,0}^\mu(\Omega) \cap J_{R,0}^\mu(\Omega)$. Then*

$$\begin{aligned} \left({}_{a_i(\mathbf{x})}^{RL} \mathcal{D}_{x_i}^\mu u, {}_{x_i}^{RL} \mathcal{D}_{b_i(\mathbf{x})}^\mu u \right) &= \cos(\mu\pi) \| {}_{-\infty}^{RL} \mathcal{D}_{x_i}^\mu \hat{u}(\mathbf{x}) \|_{L^2(\mathbb{R}^n)}^2 \\ &= \cos(\mu\pi) \| {}_{x_i}^{RL} \mathcal{D}_{+\infty}^\mu \hat{u}(\mathbf{x}) \|_{L^2(\mathbb{R}^n)}^2, \end{aligned} \quad (9)$$

where \hat{u} is the extension of u by zero outside Ω .

For fractional derivatives, we also have integration by parts formula.

Lemma 2.3 ([46, 47]). *Let $1/2 < \mu < 1$. $u, v \in H_0^\mu(\Omega) \cap H_0^{2\mu}(\Omega)$. Then*

$$\begin{aligned} \left({}_{a_i(\mathbf{x})}^{RL} \mathcal{D}_{x_i}^{2\mu} u, v \right) &= \left({}_{a_i(\mathbf{x})}^{RL} \mathcal{D}_{x_i}^\mu u, {}_{x_i}^{RL} \mathcal{D}_{b_i(\mathbf{x})}^\mu v \right), \\ \left({}_{x_i}^{RL} \mathcal{D}_{b_i(\mathbf{x})}^{2\mu} u, v \right) &= \left({}_{x_i}^{RL} \mathcal{D}_{b_i(\mathbf{x})}^\mu u, {}_{a_i(\mathbf{x})}^{RL} \mathcal{D}_{x_i}^\mu v \right). \end{aligned} \quad (10)$$

2.2. Variational forms of different derivative terms

In order to deduce suitable inner product forms for fractional derivative forms in L , we multiply those three terms by test function v separately and then apply the integration by parts formula. In the following parts of this section, assume the function u is smooth enough to apply integration by parts formula and v is zero on the boundary of Ω .

Firstly, we infer variational forms for case 1, i.e. $c(\mathbf{x})\mathcal{D}_i^{2\alpha}u(\mathbf{x})$. Assume $2\alpha = 1 + \beta$, then we have

$$\begin{aligned} (c(\mathbf{x})\mathcal{D}_i^{2\alpha}u(\mathbf{x}), v(\mathbf{x})) &= (c(\mathbf{x})\mathcal{D}_i^{1+\beta}u(\mathbf{x}), v(\mathbf{x})) \\ &= (\mathcal{D}_i^1 \mathcal{D}_i^\beta u(\mathbf{x}), c(\mathbf{x})v(\mathbf{x})) \\ &= (\mathcal{D}_i^\beta u(\mathbf{x}), \mathcal{D}_i^{1*} c(\mathbf{x})v(\mathbf{x})) \\ &= (\mathcal{D}_i^{1*} c(\mathbf{x})\mathcal{D}_i^\beta u(\mathbf{x}), v(\mathbf{x})) + (c(\mathbf{x})\mathcal{D}_i^\beta u(\mathbf{x}), \mathcal{D}_i^{1*} v(\mathbf{x})). \end{aligned} \quad (11)$$

If $c(\mathbf{x})$ is independent of x_i , by Lemma 2.3 we have

$$(c(\mathbf{x})\mathcal{D}_i^{2\alpha}u(\mathbf{x}), v(\mathbf{x})) = (c(\mathbf{x})\mathcal{D}_i^\alpha u(\mathbf{x}), \mathcal{D}_i^{\alpha*} v(\mathbf{x})), \quad (12)$$

Splitting fractional orders 2α like this is always used for dealing with Riesz fractional derivatives because it always result in a symmetrical stiffness matrix. Now, we obtain two different inner product forms for case 1.

Secondly, for case 2 and 3, we gather them together because the variational forms of them are similar. For case 2 and case 3, we can deduce them as follows

$$\left(\mathcal{D}_i(c(\mathbf{x})\mathcal{D}_i^\beta u(\mathbf{x})), v(\mathbf{x}) \right) = - (c(\mathbf{x})\mathcal{D}_i^\beta u(\mathbf{x}), \mathcal{D}_i v(\mathbf{x})). \quad (13)$$

$$\left(\mathcal{D}_i^\beta(c(\mathbf{x})\mathcal{D}_i u(\mathbf{x})), v(\mathbf{x})\right) = (c(\mathbf{x})\mathcal{D}_i u(\mathbf{x}), \mathcal{D}_i^{\beta*} v(\mathbf{x})) = (c(\mathbf{x})\mathcal{D}_i^{\beta*} v(\mathbf{x}), \mathcal{D}_i u(\mathbf{x})). \quad (14)$$

It is observed that these two terms on the right hand of (13) and (14) are actually with same form.

As demonstrated before, we have three different inner product forms listed in table 1. Obviously, they have a uniform form

$$(c(\mathbf{x})\mathcal{D}_i^\alpha u(\mathbf{x}), \mathcal{D}_i^{\beta*} v(\mathbf{x})), \quad (15)$$

where $0 \leq \alpha, \beta \leq 1$.

Table 1: Different inner product forms with fractional derivatives

Case	I	II	III
Form	$(c(\mathbf{x})\mathcal{D}_i^\beta u(\mathbf{x}), v(\mathbf{x}))$	$(c(\mathbf{x})\mathcal{D}_i^\alpha u(\mathbf{x}), \mathcal{D}_i^{\alpha*} v(\mathbf{x}))$	$(c(\mathbf{x})\mathcal{D}_i^\beta u(\mathbf{x}), \mathcal{D}_i v(\mathbf{x}))$

Remark 2.4. When $\alpha = 0$ and $\beta = 0$, form (15) will be $(u(\mathbf{x}), v(\mathbf{x}))$ which is corresponding to mass matrix.

3. Algorithms on assembling stiffness matrix

Assembling the fractional stiffness matrix is the key point to solve spatial FPDEs using FEM. In this section, we introduce algorithms related with assembling fractional stiffness matrix.

3.1. Deduction of the expression of fractional stiffness matrix

Assume the domain $\Omega \in \mathbb{R}^n$ is a polygonal domain which can be partitioned into simplexes in \mathbb{R}^n . Let $\{\mathcal{T}_h\}$ be a family of regular partitions of Ω , and h be the maximum diameter of elements in \mathcal{T}_h . For finite element methods, the idea is to approximate solutions of equations on conforming, finite dimensional spaces. So we define the test and trial space

$$V_h = \{v_h : v_h \in C(\Omega), v_h \in V, v_h|_E \in P_s(E), \forall E \in \mathcal{T}_h\}. \quad (16)$$

where $P_s(E)$ is the set of polynomials with degrees s in E .

Assume the basis functions of V_h are $\psi_l(\mathbf{x}), l = 1, 2, \dots, \mathcal{N}$. As usual, the stiffness matrix is calculated by adding the element stiffness matrices, i.e.,

$$K = \sum_{E \in \mathcal{T}_h} K_E \quad (17)$$

where K_E is element stiffness matrix with

$$(K_E)_{kl} = (c(\mathbf{x})\mathcal{D}_i^\alpha \psi_l(\mathbf{x}), \mathcal{D}_i^{\beta*} \psi_k(\mathbf{x}))_E \quad (18)$$

with $(\cdot, \cdot)_E$ representing inner product on element E .

By Gaussian quadrature on E , we can approximate $(K_E)_{kl}$ by

$$(K_E)_{kl} = \sum_{j=1}^m w_j c(\mathbf{x}_j) \mathcal{D}_i^\alpha \psi_l(\mathbf{x}_j) \mathcal{D}_i^{\beta*} \psi_k(\mathbf{x}_j) \quad (19)$$

where \mathbf{x}_j and w_j ($j = 1, 2, \dots, m$) are Gaussian points and Gaussian weights on E . In order to make the process more clear, we write $(K_E)_{kl}$ as product of matrices, i.e.

$$(K_E)_{kl} = \left(\mathcal{D}_i^{\beta*} \psi_k(\mathbf{x}_2), \mathcal{D}_i^{\beta*} \psi_k(\mathbf{x}_2), \dots, \mathcal{D}_i^{\beta*} \psi_k(\mathbf{x}_m) \right) \Lambda \begin{pmatrix} \mathcal{D}_i^\alpha \psi_l(\mathbf{x}_1) \\ \mathcal{D}_i^\alpha \psi_l(\mathbf{x}_2) \\ \vdots \\ \mathcal{D}_i^\alpha \psi_l(\mathbf{x}_m) \end{pmatrix} \quad (20)$$

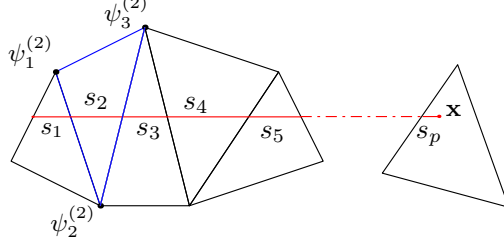


Figure 1: Integral path for Gaussian point \mathbf{x} on 2-D domain. $s_k (k = 1, 2, \dots, p)$ are the segments of the integral path. $\psi_1^{(2)}, \psi_2^{(2)}, \psi_3^{(2)}$ are local basis functions in E_2 .

where

$$\Lambda = \begin{pmatrix} w_1 c(\mathbf{x}_1) & 0 & \cdots & 0 \\ 0 & w_2 c(\mathbf{x}_2) & \cdots & 0 \\ \vdots & \vdots & \ddots & \vdots \\ 0 & 0 & \cdots & w_m c(\mathbf{x}_m) \end{pmatrix}. \quad (21)$$

Define

$$L = \begin{pmatrix} \mathcal{D}_i^\alpha \psi_1(\mathbf{x}_1) & \mathcal{D}_i^\alpha \psi_1(\mathbf{x}_2) & \cdots & \mathcal{D}_i^\alpha \psi_1(\mathbf{x}_m) \\ \mathcal{D}_i^\alpha \psi_2(\mathbf{x}_1) & \mathcal{D}_i^\alpha \psi_2(\mathbf{x}_2) & \cdots & \mathcal{D}_i^\alpha \psi_2(\mathbf{x}_m) \\ \vdots & \vdots & \ddots & \vdots \\ \mathcal{D}_i^\alpha \psi_{\mathcal{N}}(\mathbf{x}_1) & \mathcal{D}_i^\alpha \psi_{\mathcal{N}}(\mathbf{x}_2) & \cdots & \mathcal{D}_i^\alpha \psi_{\mathcal{N}}(\mathbf{x}_m) \end{pmatrix}, \quad (22)$$

and

$$R = \begin{pmatrix} \mathcal{D}_i^{\beta^*} \psi_1(\mathbf{x}_1) & \mathcal{D}_i^{\beta^*} \psi_1(\mathbf{x}_2) & \cdots & \mathcal{D}_i^{\beta^*} \psi_1(\mathbf{x}_m) \\ \mathcal{D}_i^{\beta^*} \psi_2(\mathbf{x}_1) & \mathcal{D}_i^{\beta^*} \psi_2(\mathbf{x}_2) & \cdots & \mathcal{D}_i^{\beta^*} \psi_2(\mathbf{x}_m) \\ \vdots & \vdots & \ddots & \vdots \\ \mathcal{D}_i^{\beta^*} \psi_{\mathcal{N}}(\mathbf{x}_1) & \mathcal{D}_i^{\beta^*} \psi_{\mathcal{N}}(\mathbf{x}_2) & \cdots & \mathcal{D}_i^{\beta^*} \psi_{\mathcal{N}}(\mathbf{x}_m) \end{pmatrix}. \quad (23)$$

Then we have

$$K_E = R \Lambda L^T. \quad (24)$$

If we denote \mathbf{l}_j and \mathbf{r}_j as the j^{th} column of L and R separately. K_E can be written as

$$K_E = \sum_{j=1}^m w_j c(\mathbf{x}_j) \mathbf{r}_j \mathbf{l}_j^T. \quad (25)$$

Remark 3.1. From above deduction, we notice that the element stiffness matrix K_E for fractional partial differential equations can not be calculated locally. This is very different with the integer case.

How to compute \mathbf{l}_j and \mathbf{r}_j is what we need consider next. Here we take \mathbf{l}_j as an example, and \mathbf{r}_j can be calculated by the same way. In order to make it clear, the subscript j is dropped in the followings. Assume \mathcal{D}_i^α is left Riemann-Liouville fractional operator. Assume we have find the integral path for Gaussian point \mathbf{x} (This will be discussed in following sections). Denote $s_k (k = 1, 2, \dots, p)$ the segments of the integral path, see Figure. And assume s_k is in element E_k . Then we have

$$\begin{aligned} \mathcal{D}_i^\alpha \psi_l(\mathbf{x}) &= \frac{1}{\Gamma(1-\alpha)} \frac{d}{dx_i} \int_{a_i(\mathbf{x})}^{x_i} (x_i - y_i)^{-\alpha} \psi_l(\mathbf{y}) dy_i \\ &= \frac{1}{\Gamma(1-\alpha)} \frac{d}{dx_i} \sum_{k=1}^p \int_{s_k} (x_i - y_i)^{-\alpha} \psi_l(\mathbf{y}) dy_i \\ &= \frac{1}{\Gamma(1-\alpha)} \sum_{k=1}^p \frac{d}{dx_i} \int_{s_k} (x_i - y_i)^{-\alpha} \psi_l(\mathbf{y}) dy_i \end{aligned} \quad (26)$$

where $\mathbf{y} = \mathbf{x} + (y_i - x_i) \mathbf{e}_i$.

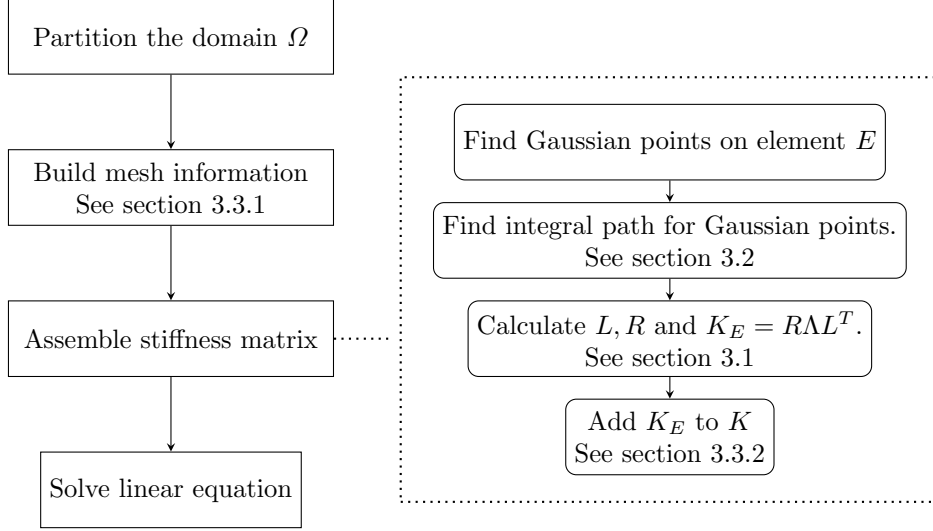


Figure 2: The big picture of solving spatial FPDEs by FEM

Define a discrete operator

$$\mathcal{D}_{i,s_k}^\alpha \psi_l(\mathbf{x}) := \frac{1}{\Gamma(1-\alpha)} \frac{d}{dx_i} \int_{s_k} (x_i - y_i)^{-\alpha} \psi_l(\mathbf{y}) dy_i. \quad (27)$$

Then, obviously, we have

$$\mathcal{D}_i^\alpha \psi_l(\mathbf{x}) = \sum_{k=1}^p \mathcal{D}_{i,s_k}^\alpha \psi_l(\mathbf{x}) \quad (28)$$

Hence

$$\mathbf{1} = \sum_{k=1}^p (\mathcal{D}_{i,s_k}^\alpha \psi_1(\mathbf{x}), \mathcal{D}_{i,s_k}^\alpha \psi_2(\mathbf{x}), \dots, \mathcal{D}_{i,s_k}^\alpha \psi_N(\mathbf{x}))^T =: \sum_{k=1}^p \mathbf{1}^{(k)} \quad (29)$$

From the definition of $\mathcal{D}_{i,s_k}^\alpha \psi_l(\mathbf{x})$, we can deduce that if ψ_l is not a local basis function on E_k , i.e. ψ_l is zero on s_k , we have $\mathcal{D}_{i,s_k}^\alpha \psi_l(\mathbf{x}) = 0$. Therefore, $\mathbf{1}^{(k)}$ is very sparse and it can be got by only computing $\mathcal{D}_{i,s_k}^\alpha \psi_l^{(k)}(\mathbf{x})$ where $\psi_l^{(k)}(l = 1, 2, \dots, n+1)$ are local basis functions on E_k . By this way we can calculate $\mathbf{1}$ locally and the process of computing $\mathbf{1}$ will similar with the idea of assembling stiffness matrix for integer case.

As a conclusion, we sketch the big picture of solving spatial FPDEs by FEM in fig. 2. This procedure is similar with the algorithm for integer order partial differential equations except for building mesh information and assembling stiffness matrix. These aspects will be addressed in following subsections.

Remark 3.2. We can calculate $\mathcal{D}_{i,s_k}^\alpha \psi_l^{(k)}(\mathbf{x})$ by Gaussian quadrature formula. But, analytical calculation of it is more efficient, see [46, Section 3.2] for more details.

Remark 3.3. Computing the numerical values of inner products, we use tetrahedral quadrature formulas[29]. The formulas are effective for polynomials with integer degree, but for fractional derivatives of polynomials it is less effective. The reason is that the fractional derivatives of polynomials are usually polynomials with non-integer degree. Due to this, when $c(\mathbf{x})$ is constant, the two equivalent inner forms of Case 1 will have different numerical results. The higher order of quadrature formulas we use, the more close the results are. Owing to this, how to compute the inner product accurately is what we will study in the future.

3.2. Find the integration path for Gaussian point

Currently, most algorithms used for searching the integration paths are exhaustive, i.e. computing the intersection segments of the ray with most of elements, even every element in the mesh. In [46], we introduced the effect domain to reduce the computation time. Here, we provide another way to accelerate the computation by the ray-simplex intersection algorithm.

3.2.1. The ray-simplex intersection algorithm

We now turn to the algorithm of ray-simplex intersection. The main idea of this algorithm is representing the ray in a new coordinate system related to the simplex[22, Chapter 2].

Let the ray and the simplex be R and S , separately. Assume the vertexes of simplex S are $\mathbf{v}_i (i = 0, \dots, n)$. Then set $\tilde{\mathbf{e}}_i = \mathbf{v}_i - \mathbf{v}_0 (i = 1, \dots, n)$. It is easily to see that $\{\tilde{\mathbf{e}}_i\}_{i=1}^n$ forms a basis for \mathbb{R}^n . Hence, every point in simplex S can be expressed as

$$\mathbf{x} = \mathbf{v}_0 + k_1 \tilde{\mathbf{e}}_1 + k_2 \tilde{\mathbf{e}}_2 + \dots + k_n \tilde{\mathbf{e}}_n, \quad (30)$$

where

$$\begin{cases} k_i \geq 0, \\ k_0 := 1 - \sum_{i=1}^n k_i \geq 0. \end{cases} \quad (31)$$

If we set $\tilde{\mathbf{k}} = (k_0, k_1, \dots, k_n)^T$, then $\tilde{\mathbf{k}}$ is the volume coordinate of \mathbf{x} in the simplex. Let \mathbf{u}_0 be the start point of R and $\mathbf{d} (|\mathbf{d}| = 1)$ be the direction of R , then every point on ray R can be written as

$$\mathbf{x} = \mathbf{u}_0 + r\mathbf{d}, \quad r \geq 0. \quad (32)$$

Let $A = (\tilde{\mathbf{e}}_1, \tilde{\mathbf{e}}_2, \dots, \tilde{\mathbf{e}}_n)$, $\mathbf{k} = (k_1, k_2, \dots, k_n)^T$, $\mathbf{b} = \mathbf{u}_0 - \mathbf{v}_0$. If \mathbf{x} is an intersection point of S and R , then we have

$$A\mathbf{k} = \mathbf{b} + r\mathbf{d}, \quad r \geq 0, \quad k_i \geq 0 \quad (i = 1, 2, \dots, n).$$

i.e.

$$\mathbf{k} = A^{-1}\mathbf{b} + rA^{-1}\mathbf{d}, \quad r \geq 0, \quad k_i \geq 0 \quad (i = 1, 2, \dots, n). \quad (33)$$

Inserting (33) into (31), we obtain the intersection conditions only including unknown variable r as below

$$\begin{cases} r \geq 0, \\ \tilde{\mathbf{b}} + r\tilde{\mathbf{d}} \geq \mathbf{0}, \end{cases} \quad (34)$$

where the operator ' \geq ' is element-wise and

$$\tilde{\mathbf{b}} = \begin{pmatrix} A^{-1}\mathbf{b} \\ 1 - \mathbf{e}^T A^{-1}\mathbf{b} \end{pmatrix}, \quad \tilde{\mathbf{d}} = \begin{pmatrix} A^{-1}\mathbf{d} \\ \mathbf{e}^T A^{-1}\mathbf{d} \end{pmatrix} \quad (35)$$

with \mathbf{e} is a n -D column vector with every element equal to 1.

Now, the intersection segment can be derived by solving inequalities (34). Actually, we only need to know the maximum and the minimum r satisfying (34). Let I be the set of all r satisfied equation (34). If I is empty, the ray and the simplex is separated. Otherwise I is an interval, i.e. $I = [r_{\min}, r_{\max}]$, $r_{\min} \leq r_{\max}$. Therefor, the two end points of the intersection segment are

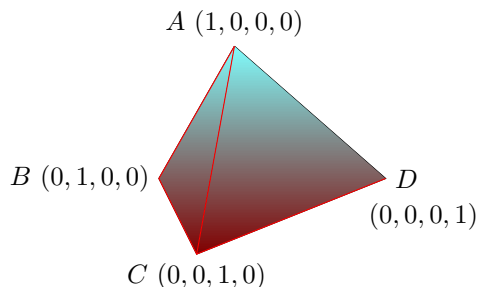
$$\mathbf{x}_0 = \mathbf{v}_0 + r_{\min}\mathbf{d}, \quad \mathbf{x}_1 = \mathbf{v}_0 + r_{\max}\mathbf{d}, \quad (36)$$

where \mathbf{x}_1 is the go-out point of R from simplex S . In addition, the volume coordinates of \mathbf{x}_0 and \mathbf{x}_1 can be written as

$$\tilde{\mathbf{k}}_{\min} = \tilde{\mathbf{b}} + r_{\min}\tilde{\mathbf{d}}, \quad \tilde{\mathbf{k}}_{\max} = \tilde{\mathbf{b}} + r_{\max}\tilde{\mathbf{d}}. \quad (37)$$

Now, the ray-simplex intersection algorithm has been introduced. In the next, we will use this algorithm to search integral paths from Gaussian points. As a conclusion, we summarize the advantages of this algorithm below.

- a) It can be used to compute the intersection points of ray and simplex in arbitrary dimensions.
- b) It avoid searching the intersection points of ray and faces of simplex by computing intersection points of ray and faces of simplex one by one.
- c) We can easily get the volume coordinates of the intersection points, which are useful in computing the fractional derivatives of basis in finite element space. From the zeros and their distribution in volume coordinates, we can easily know where the intersection is, see fig. 3. Using this fact, we can find the path of integration more efficiently.



Position of Points	Volume Coordinates
AB	$(k_1, k_2, 0, 0)$.
AC	$(k_1, 0, k_3, 0)$.
AD	$(k_1, 0, 0, k_4)$.
BC	$(0, k_2, k_3, 0)$.
CD	$(0, 0, k_3, k_4)$.
Δ_{ABC}	$(k_1, k_2, k_3, 0)$.
Δ_{ABD}	$(k_1, k_2, 0, k_4)$.
Δ_{ACD}	$(k_2, 0, k_3, k_4)$.
Δ_{BCD}	$(0, k_2, k_3, k_4)$.

Figure 3: The volume coordinates of nodes and points on edges and faces in tetrahedron.

3.2.2. Applied ray-simplex algorithms to find the integration path

Assume we have known the adjacent information of the triangulation. If a ray intersects with a simplex Δ , then it must go out from some point on some m -face ($0 \leq m < n, m \in \mathbb{N}$) of the simplex Δ , for example, edge(1-face), vertex(0-face) in 2-D case, and face(2-face), edge(1-face), vertex(0-face) in 3-D case. By the volume coordinate of the go-out point, we can deduce the simplex with which the ray maybe intersection after going out of current simplex. *If the volume coordinate of one point has k zero components, then the point must be on some $(n - k)$ -face of the simplex. And the exact face can be determined by the distribution of the zero components of the volume coordinate, see fig. 3 for 3-D case.* If the go-out point is on a m -face, we can search all the elements (simplex) which contain the m -face. Usually, most of the go-out points will locate on $(n - 1)$ -face of the simplex Δ , for example, edges in 2-D and faces in 3-D (See fig. 4). And in this situation, there are at most one simplex shared the face with simplex Δ . This is why this algorithm is efficient.

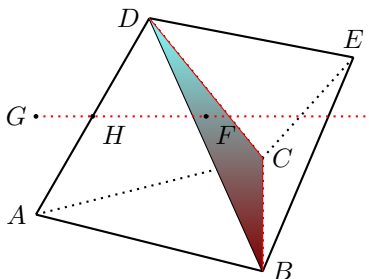


Figure 4: An example show the integration path in two elements Δ_{ABCD} and Δ_{BCDE} . The integration path GH go out at point F from Δ_{ABCD} , then we can assure that GH must go into Δ_{BCDE} at F because F is on face BCD .

As a conclusion of this subsection, the algorithm of finding integration paths is given in algorithm 1. As long as we know the integration paths, we can compute the fractional derivatives at Gaussian points by the way provided in Section 3.1.

Remark 3.4. By the description above, we notice that the adjacent information must include the m -face to element relationship, i.e., given a m -face we can get all elements sharing this face together. This information should be gathered before the procedure of finding integration paths.

3.3. Some details on implementations

To make the algorithms more clear, here we give more details on the implementation in 3-D case.

3.3.1. Some implementation details of finding integral path

In this subsection, we consider the data structure of the mesh and how to use this information in finding integral path. The basic information of a mesh including points (or called nodes, vertex) and cells (or called

Algorithm 1 Finding the integral path

Require: Gaussian points G in simplex Δ , Adjacent information I .

Require: Ray R start from G with direction \mathbf{d} .

```

1: Simplex set  $S \leftarrow \{\Delta\}$ ;
2: Simplex and segment pair set  $P \leftarrow \emptyset$ ;
3:  $flag \leftarrow 0$ ;
4: for Each simplex  $\Delta'$  in  $S$  do
5:   Compute the ray's in- and out-points pair  $(\mathbf{k}_0, \mathbf{k}_1)$  with  $\Delta'$ ;
6:   if in- and out-points is not the same point then
7:      $flag \leftarrow 1$ ;
8:     Current simplex  $\Delta_c \leftarrow \Delta'$ ;
9:     go to 12;
10:  end if
11: end for
12: if  $flag = 1$  then
13:   Put simplex and segment pair  $\{\Delta_c, (\mathbf{k}_0, \mathbf{k}_1)\}$  in  $P$ ;
14:   Determine the face  $F$  by out-points  $\mathbf{k}_1$ ;
15:   Get the simplex set  $S'$  of which the element shared the face  $F$ ;
16:    $S \leftarrow S' - \{\Delta_c\}$ ;
17:   go to 3;
18: end if
19: return  $P$ 

```

Table 2: Information of nodes

Index	1	2	\dots	i	\dots	N
	x_1	x_2	\dots	x_i	\dots	x_N
Nodes	y_1	y_2	\dots	y_i	\dots	y_N
	z_1	z_2	\dots	z_i	\dots	z_N

Table 3: Information of cells

Index	1	2	\dots	i	\dots	M
	$E_1(1)$	$E_2(1)$	\dots	$E_i(1)$	\dots	$E_M(1)$
Cells	$E_1(2)$	$E_2(2)$	\dots	$E_i(2)$	\dots	$E_M(2)$
	$E_1(3)$	$E_2(3)$	\dots	$E_i(3)$	\dots	$E_M(3)$
	$E_1(4)$	$E_2(4)$	\dots	$E_i(4)$	\dots	$E_M(4)$

elements). The nodes are stored in a matrix of which each column represents a point as shown in table 2. The elements are also stored in a matrix shown in table 3 where $E_i(j)$ is the index of the corresponding nodes, i.e. the index of the j^{th} nodes in cell E_i . If we define local nodes index set $I_l = \{1, 2, 3, 4\}$ and global nodes index set $I_n = \{1, 2, \dots, N\}$, E_i can be seen as a map from I_l to I_n . So the matrix of cells actually stores the map E_i .

Table 4: Information of edges where e_i is a map from $\{1, 2\}$ to I_n .

Index	1	2	\dots	i	\dots	N_e
Edges	$e_1(1)$	$e_2(1)$	\dots	$e_i(1)$	\dots	$e_{N_e}(1)$
	$e_1(2)$	$e_2(2)$	\dots	$e_i(2)$	\dots	$e_{N_e}(2)$

From this basic information, we can get all the edges and faces in this mesh, and they are shown in table 4 and 5.

As state before, we need the adjacency information of the mesh, such as cells to edges and edges to cells. Define edges index set $I_e = \{1, 2, \dots, N_e\}$ and faces index set $I_f = \{1, 2, \dots, N_f\}$. Denote $I_l^{(i)}$ as the set

Table 5: Information of faces where f_i is a map from $\{1, 2, 3\}$ to I_n .

Index	1	2	...	i	...	N_f
Faces	$f_1(1)$	$f_2(1)$...	$f_i(1)$...	$f_{N_f}(1)$
	$f_1(2)$	$f_2(2)$...	$f_i(2)$...	$f_{N_f}(2)$
	$f_1(3)$	$f_2(3)$...	$f_i(3)$...	$f_{N_f}(3)$

of subsets of I_l with i elements, i.e. $I_l^{(2)} = \{\{1, 2\}, \{1, 3\}, \{1, 4\}, \{2, 3\}, \{2, 4\}, \{3, 4\}\}$. Define map E_i on $I_l^{(2)}$ and $I_l^{(3)}$ as follows.

$$E_i : I_l^{(2)} \rightarrow I_e, \quad E_i : I_l^{(3)} \rightarrow I_f. \quad (38)$$

Here we use symbol E_i again, because it represent a map from local index to global index. This will not introduce any confusion because they are defined on different index sets. These two maps are shown in table 6 and 7. This information is not enough for assembling stiffness matrix. We need more. Define map

Table 6: Edges of cells where E_i is a map from $I_l^{(2)}$ to I_e .

Index	1	2	...	i	...	M
Edges of cells	$E_1(1, 2)$	$E_2(1, 2)$...	$E_i(1, 2)$...	$E_M(1, 2)$
	$E_1(1, 3)$	$E_2(1, 3)$...	$E_i(1, 3)$...	$E_M(1, 3)$
	$E_1(1, 4)$	$E_2(1, 4)$...	$E_i(1, 4)$...	$E_M(1, 4)$
	$E_1(2, 3)$	$E_2(2, 3)$...	$E_i(2, 3)$...	$E_M(2, 3)$
	$E_1(2, 4)$	$E_2(2, 4)$...	$E_i(2, 4)$...	$E_M(2, 4)$
	$E_1(3, 4)$	$E_2(3, 4)$...	$E_i(3, 4)$...	$E_M(3, 4)$

Table 7: Faces of cells where E_i is a map from $I_l^{(3)}$ to I_e .

Index	1	2	...	i	...	M
Faces of cells	$E_1(1, 2, 3)$	$E_2(1, 2, 3)$...	$E_i(1, 2, 3)$...	$E_M(1, 2, 3)$
	$E_1(1, 2, 4)$	$E_2(1, 2, 4)$...	$E_i(1, 2, 4)$...	$E_M(1, 2, 4)$
	$E_1(1, 3, 4)$	$E_2(1, 3, 4)$...	$E_i(1, 3, 4)$...	$E_M(1, 3, 4)$
	$E_1(2, 3, 4)$	$E_2(2, 3, 4)$...	$E_i(2, 3, 4)$...	$E_M(2, 3, 4)$

$$E^{(n)} : I_n \rightarrow 2^{I_E}, \quad E^{(e)} : I_e \rightarrow 2^{I_E}, \quad E^{(f)} : I_f \rightarrow 2^{I_E}. \quad (39)$$

where $E^{(e)}$ map an index of edge to the index of cells containing this edge and $E^{(f)}$ maps an index of face to the index of cells containing this face. Tables 8 to 10 show the structure of $E^{(n)}$, $E^{(e)}$ and $E^{(f)}$.

Table 8: Adjacency information of nodes to cells

Index	1	2	...	i	...	N
Nodes to cells	$E^n(1)$	$E^n(2)$...	$E^n(i)$...	$E^n(N)$

Table 9: Adjacency information of edges to cells

Index	1	2	...	i	...	N_e
Edges to cells	$E^e(1)$	$E^e(2)$...	$E^e(i)$...	$E^e(N_e)$

These are all the information of the mesh we need. Now we state how to find the position of a points from its volume coordinate as we need this when find the integral path. Assume we have a point P in E_i , and its volume coordinate is $\mathbf{k} = (k_1, k_2, k_3, k_4)$. According to fig. 3 which showing the relationship of volume coordinate with its position, we have some proposition as below.

Table 10: Adjacency information of faces to cells

Index	1	2	...	i	...	N_f
Faces to cells	$E^f(1)$	$E^f(2)$...	$E^f(i)$...	$E^f(N_f)$

- a) When there are three zeros in \mathbf{k} and the non-zero element's subscript is j , i.e. $k_j \neq 0$, then $E_i(j)$ is P . Then $E^n(E_i(j))$ contain all the cells share the point P .
- b) When there are two zeros in \mathbf{k} and the subscripts are j_1, j_2 , then P is on edge $E_i(j_1, j_2)$. Then $E^e(E_i(j_1, j_2))$ contain all the cells share the point P .
- c) When there is one zero in \mathbf{k} and the non-zero elements' subscripts are j_1, j_2, j_3 , then P is on face $E_i(j_1, j_2, j_3)$. Then $E^f(E_i(j_1, j_2, j_3))$ contain all the cells share the point P .

These facts are used in algorithm 1 to speedup the procedure of finding integral path, see Line 14-15 in the algorithm.

Remark 3.5. As mentioned before, we need to check the distribution of zero components in volume coordinates of intersection points. However, we seldom get exact zeros in computers. So a suitable tolerance must be set, for example $\text{tol} = 10^{-12}$.

3.3.2. Speedup addition of sparse matrix in MATLAB

In this subsection, we exploit the sparsity of the fractional stiffness matrix and make use of the sparsity to speed up the procedure of assembling fractional stiffness matrix.

Here we take equations with Riesz fractional derivatives as an example. Suppose we have a cubic domain with uniform grid in \mathbb{R}^n and assume we have N grid points on each direction. Then, when $n = 1$, the stiffness matrix is full. if $n > 1$, the matrix is a sparse matrix and the density of the matrix is proportional to $1/N^{n-1}$. This can be got easily by simple calculation. In order to compare the sparsity of fractional stiffness matrix with traditional stiffness matrix, we list the density of them in table 11. In MATLAB, we can visualize sparsity pattern of a sparse matrix by command `spy`. In fig. 5, we show the sparsity pattern of a fractional stiffness matrix K . The density of this matrix is 2.7%. Though the subfigure (a) in fig. 5 seems an full matrix, the sparsity of K is obvious after we zoom in the figure as shown in subfigure (c) and (d).

Table 11: Density of the stiffness matrix in different dimensions.

Type	1-D	2-D	3-D
Traditional Equ.	$O(1/N)$	$O(1/N^2)$	$O(1/N^3)$
Fractional Equ.	1	$O(1/N)$	$O(1/N^2)$

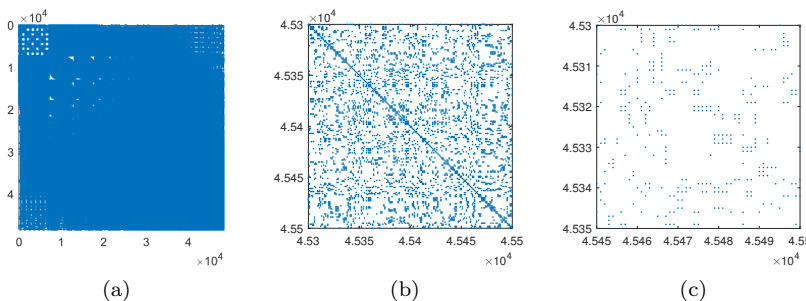


Figure 5: Distribution of non-zero elements in fractional stiffness matrix $K_{48456 \times 48456}$ with density 2.7%. (a) K ; (b) $K(45300 : 45500, 45300 : 45500)$; (c) $K(45350 : 45500, 45350 : 45500)$.

When assembling the stiffness matrix we need to add element stiffness matrices together. However, this operation will cost much CPU time because of the sparse matrix storage method in MATLAB. To accelerate

the operation, we firstly construct a sparse matrix, called template matrix, of which the structure is 'similar' with the result matrix K . Then add sparse matrices by a C routine in place. This will save a lot of time.

Now we briefly describe the idea of constructing the template matrix T . Assume $K_{\mathcal{N} \times \mathcal{N}}$ is a fractional stiffness matrix. Then we define template matrix T of K as below

$$T_{jk} = \begin{cases} 0, & \text{if } K_{jk} = 0, \\ 1, & \text{if } K_{jk} \neq 0. \end{cases} \quad (40)$$

So, the process of constructing T is actually to determine whether K_{jk} is zero. Here, we take $(c_i(\mathbf{x})\mathcal{D}_i^\alpha u(\mathbf{x}), \mathcal{D}_i^{\beta^*} v(\mathbf{x}))$ as an example, i.e. $K_{jk} = (c_i(\mathbf{x})\mathcal{D}_i^\alpha \phi_k(\mathbf{x}), \mathcal{D}_i^{\beta^*} \phi_j(\mathbf{x}))$ where $j, k \in \{1, 2, \dots, \mathcal{N}\}$. As linear Lagrange element is used, we assume the vertex corresponding to basis function $\phi_j(\mathbf{x})$ is \mathbf{z}_j and define ω_j as the element patch of \mathbf{z}_j , i.e. $\omega_j = \cup_{\mathbf{z}_j \in E} E$. Define the lower and upper bound of ω_j in \mathbf{e}_i direction as

$$\begin{cases} z_{j,min}^{(i)} = \min\{x_i | \mathbf{x} \in \omega_j\}, \\ z_{j,max}^{(i)} = \max\{x_i | \mathbf{x} \in \omega_j\}. \end{cases} \quad (41)$$

According to the definition of fractional derivatives, if

$$[z_{j,min}^{(i)}, z_{j,max}^{(i)}] \cap [z_{k,min}^{(i)}, z_{k,max}^{(i)}] = \emptyset,$$

the element K_{jk} and K_{kj} must be zeros, i.e. $T_{jk} = T_{kj} = 0$. Otherwise, K_{jk} and K_{kj} are non-zero, i.e. $T_{jk} = T_{kj} = 1$.

The efficiency of this algorithm can be seen from table 12 and fig. 6, which shows time cost of MATLAB build-in function 'plus' and C routine 'addsparse' in assembling the stiffness matrix of Riesz fractional derivatives. For traditional stiffness matrix ($\alpha = 1$), There is not much difference between the two methods. But the 'addsparse' has a lower rate of increase. For fractional stiffness matrix, the acceleration effect of 'addsparse' is remarkable. In addition, the readers can find the C routine at <https://github.com/lrtfm/addsparse>.

Table 12: Compare of times cost by MATLAB build-in function 'plus' and our C routine 'addsparse'.

Number of elements	$\alpha = 1$		$\alpha = 0.8$	
	'addsparse'	'plus'	'addsparse'	'plus'
940	0.06s	0.03s	0.07s	0.07s
2583	0.18s	0.13s	0.29s	0.62s
7836	0.71s	0.89s	1.12s	7.69s
10746	1.05s	1.52s	1.73s	50.40s
15933	1.87s	3.23s	2.95s	125.61s
22643	3.22s	6.29s	5.12s	284.18s
38139	7.52s	20.09s	11.62s	945.53s

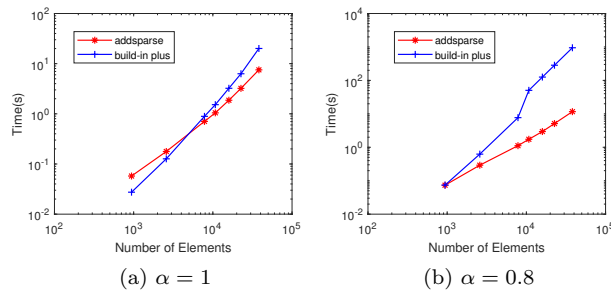


Figure 6: Compare of times cost by MATLAB build-in function 'plus' and our C routine 'addsparse'.

As a conclusion of this section, we present the algorithm on assembling fractional stiffness matrix in algorithm 2.

Algorithm 2 Assemble the fractional stiffness matrix

Require: Triangulation \mathcal{T} , Element $E \in \mathcal{T}$, Matrix $K \leftarrow \mathbf{0}$.

Require: Basis function $\psi_l(\mathbf{x}), l = 1, 2, \dots, \mathcal{N}$ on triangulation \mathcal{T}

- 1: Construct template matrix T for K .
 - 2: $K \leftarrow T$.
 - 3: **for** each element $E \in \mathcal{T}$ **do**
 - 4: Get Gaussian points G_E and associated weights on E
 - 5: **for** each Gaussian point $P_j \in G_E$ with weight w_j **do**
 - 6: Let \mathbf{x} be the coordinates of P_j .
 - 7: Calculate vector $\mathbf{l}_j \leftarrow (\mathcal{D}_i^\alpha \psi_1(\mathbf{x}), \mathcal{D}_i^\alpha \psi_2(\mathbf{x}), \dots, \mathcal{D}_i^\alpha \psi_{\mathcal{N}}(\mathbf{x}))^T$.
 - 8: Calculate vector $\mathbf{r}_j \leftarrow (\mathcal{D}_i^{\beta^*} \psi_1(\mathbf{x}), \mathcal{D}_i^{\beta^*} \psi_2(\mathbf{x}), \dots, \mathcal{D}_i^{\beta^*} \psi_{\mathcal{N}}(\mathbf{x}))^T$.
 - 9: Calculate $c_j \leftarrow c_i(\mathbf{x})$.
 - 10: **end for**
 - 11: Assemble the element stiffness matrix $K_E \leftarrow \sum_j w_j c_j \mathbf{r}_j \mathbf{l}_j^T$.
 - 12: $K \leftarrow \text{addsparse}(K, K_E)$.
 - 13: **end for**
 - 14: $K \leftarrow K - T$.
 - 15: **return** K
-

4. Applications

4.1. Application to steady fractional diffusion equations

Example 4.1. Consider FPDEs with left Riemann-Liouville fractional derivatives

$$\begin{cases} \sum_{i=1}^3 p_i {}^{\text{RL}}\mathcal{D}_{x_i}^{2\alpha_i} u(\mathbf{x}) = f(\mathbf{x}), & \mathbf{x} \in \Omega, \\ u(\mathbf{x}) = 0, & \mathbf{x} \in \Omega^c, \end{cases} \quad (42)$$

where $1/2 < \alpha_i < 1$, $\Omega = (0, 1) \times (0, 1) \times (0, 1)$ and $p_i (i = 1, 2, 3)$ are constants.

The variational form of this problem can be written as $a(u, v) = (f, v)$, where, as talked before, the bilinear form $a(u, v)$ have two forms, i.e.

$$a(u, v) = \sum_{i=1}^3 p_i \left({}^{\text{RL}}\mathcal{D}_{x_i}^{\alpha_i} u, {}^{\text{RL}}\mathcal{D}_{b_i(\mathbf{x})}^{\alpha_i} v \right), \quad (43)$$

and

$$a(u, v) = \sum_{i=1}^3 -p_i \left({}^{\text{RL}}\mathcal{D}_{x_i}^{2\alpha_i-1} u, \mathcal{D}_i v \right). \quad (44)$$

Now, we perform numerical experiments to compare results of the two variational forms. Denote $p := (p_1, p_2, p_3)$, $\alpha := (\alpha_1, \alpha_2, \alpha_3)$. Let $p = (1, 1, 1)$, $\alpha = (0.85, 0.85, 0.85)$ and the exact solution of (42) be

$$u(\mathbf{x}, t) = 2^9 x_1^2 x_2^2 x_3^2 (x_1 - 1)(x_2 - 1)(x_3 - 1). \quad (45)$$

Then the right hand function $f(\mathbf{x})$ can be obtained by inserting $u(\mathbf{x}, t)$ into equation (42).

Firstly, we solve equation (42) by using bilinear form (43). The meshes are shown in fig. 7, and L^2 , L^∞ errors and convergence orders are shown in table 13. In order to compare the numerical results with exact solution, we choose a plane and a line on the domain and plot the numerical results and exact solution at the same time. In fig. 8, the numerical result and the exact solution are shown in filled contour plots. As shown in the figure, the numerical result is almost same with the exact solution when $h = 1/32$. In fig. 9, we depict the numerical results and errors on line $x_2 = 1/2, x_3 = 1/2$. It is easily to see that the method is convergence as we refine the mesh. Then, we resolve the equation by form (44). The errors and convergence orders are shown in table 13. The numerical results on a line are illustrated in fig. 10. In table 13, we notice

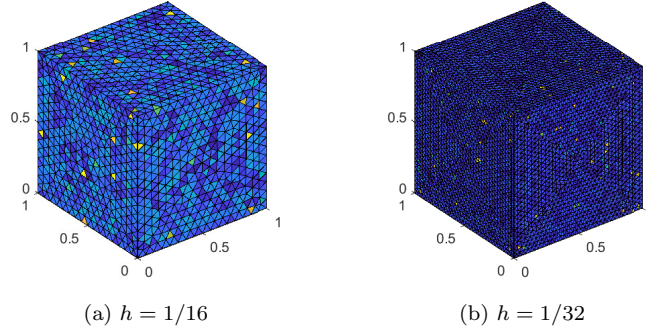


Figure 7: Meshes on a cubic with different sizes.

Table 13: L^2 and L^∞ errors and convergence order

$a(u, v)$	h	$\ u - u_h\ _{L^2}$	order	$\ u - u_h\ _{L^\infty}$	order
Form (43)	1/16	1.62e-02		4.89e-02	
	1/25	7.40e-03	1.75	2.28e-02	1.71
	1/32	4.91e-03	1.67	1.55e-02	1.57
Form (44)	1/16	1.52e-02		4.75e-02	
	1/25	6.83e-03	1.80	2.20e-02	1.73
	1/32	4.45e-03	1.73	1.47e-02	1.63

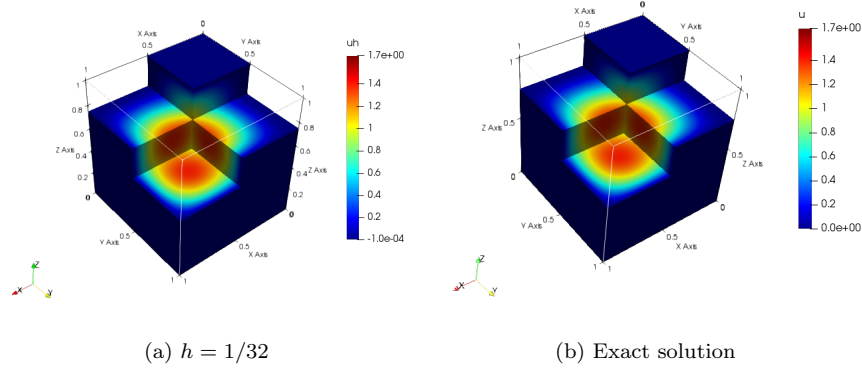


Figure 8: Numerical results of equation (42) by using bilinear form (43) and exact solution.

that the results of the two forms have a tiny difference which can be ignored. Hence, when these two form are available at the same time, anyone of them can be used to solve the equation. Usually, we choose form (44) because it is more efficient.

Example 4.2. In this example, we solve steady fractional diffusion equations with variable coefficients on domain $\Omega = (0, 1) \times (0, 1) \times (0, 1)$. Consider FPDEs with variable coefficients in divergence form

$$\begin{cases} \sum_{i=1}^3 \mathcal{D}_i \left(p_i(\mathbf{x}) {}_{a_i(\mathbf{x})}^{\text{RL}} \mathcal{D}_{x_i}^{\beta_i} u(\mathbf{x}) - q_i(\mathbf{x}) {}_{x_i}^{\text{RL}} \mathcal{D}_{b_i(\mathbf{x})}^{\beta_i} u(\mathbf{x}) \right) = f(\mathbf{x}), & \mathbf{x} \in \Omega, \\ u(\mathbf{x}) = 0, & \mathbf{x} \in \Omega^c. \end{cases} \quad (46)$$

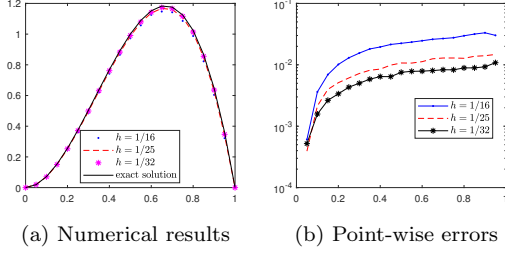


Figure 9: Numerical results and point-wise errors of equation (42) by using form (43) on line $x_2 = 1/2, x_3 = 1/2$.

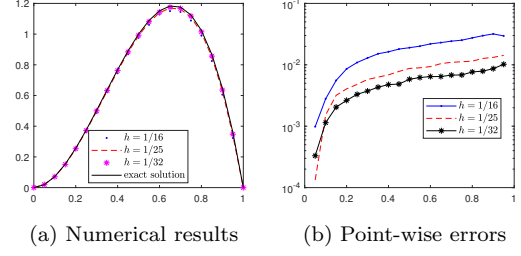


Figure 10: Numerical results and point-wise errors of equation (42) by using form (44) on line $x_2 = 1/2, x_3 = 1/2$.

where $p_i > 0, q_i > 0$. The variational form of this equation is $a(u, v) = (f, v)$ where

$$a(u, v) = - \sum_{i=1}^3 \left((p_i(\mathbf{x}) {}_{a_i(\mathbf{x})}^{\text{RL}} \mathcal{D}_{x_i}^{\beta_i} u, \mathcal{D}_i v) - (q_i(\mathbf{x}) {}_{x_i}^{\text{RL}} \mathcal{D}_{b_i(\mathbf{x})}^{\beta_i} u, \mathcal{D}_i v) \right). \quad (47)$$

Denote $\beta := (\beta_1, \beta_2, \beta_3)$. Set $p(\mathbf{x}) = (x_1, x_2, x_3), q(\mathbf{x}) = (1 - x_1, 1 - x_2, 1 - x_3)$. And let the exact solution be

$$u(\mathbf{x}) = 2^{12} x_1^2 x_2^2 x_3^2 (x_1 - 1)^2 (x_2 - 1)^2 (x_3 - 1)^2. \quad (48)$$

Then, solve the equation by using algorithm presented in Section 3. The errors and convergence orders are shown in table 14. The convergence orders of L^2 and L^∞ errors are bigger than 1.5. Also, we plot the results and errors on line $x_2 = 1/2, x_3 = 1/2$ in fig. 11 and 12. From these tables and figures, it is easily to see that our method is convergence.

Table 14: L^2 and L^∞ errors and convergence order for equation (46).

β	h	$\ u - u_h\ _{L^2}$	order	$\ u - u_h\ _{L^\infty}$	order
(0.8, 0.8, 0.8)	1/16	6.46e-03		1.74e-02	
	1/20	4.38e-03	1.75	1.20e-02	1.65
	1/32	1.91e-03	1.77	5.45e-03	1.68
(0.6, 0.7, 0.8)	1/16	7.26e-03		1.86e-02	
	1/20	4.99e-03	1.67	1.30e-02	1.60
	1/32	2.24e-03	1.70	6.29e-03	1.55

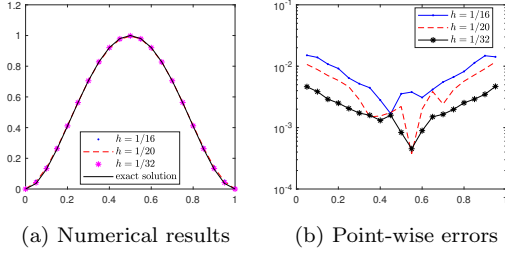


Figure 11: Numerical results on line $x_2 = 1/2, x_3 = 1/2$ when $\beta = (0.8, 0.8, 0.8)$.

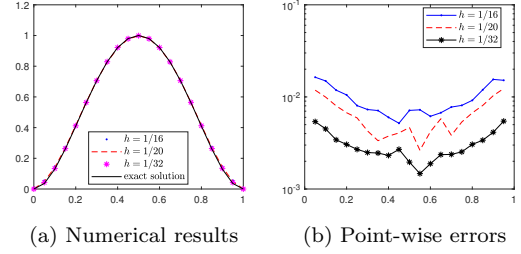


Figure 12: Numerical results on line $x_2 = 1/2, x_3 = 1/2$ when $\alpha = (0.6, 0.7, 0.8)$.

4.2. Application to fractional diffusion equations

In this subsection, we consider time-dependent FPDEs in general form firstly, and then consider a special case with Riesz fractional operators. Firstly, let us define some notations. Denote τ the time step size

and n_T a positive integer with $\tau = T/n_T$. And let $t_{j-\frac{1}{2}} = (j - \frac{1}{2})\tau$ for $j = 1, 2, \dots, n_T$. For functions $u(\mathbf{x}, t)$ and $f(\mathbf{x}, t)$, denote $u^j = u^j(\cdot) = u(\cdot, t_j)$, $u^{j-\frac{1}{2}} = \frac{1}{2}(u^j + u^{j-1})$, $f^j = f(\cdot, t_j)$, $f^{j-\frac{1}{2}} = f(\cdot, t_{j-\frac{1}{2}})$, and $\bar{\partial}_t u^j = \frac{u^j - u^{j-1}}{\tau}$.

4.2.1. General case

In this subsection, we consider time-dependent FPDEs as follows

$$\begin{cases} \frac{\partial u}{\partial t} = \sum_{i=1}^3 \mathcal{D}_i \left(p_i(\mathbf{x}) {}_{a_i(\mathbf{x})}^{\text{RL}} \mathcal{D}_{x_i}^{\beta_i} u(\mathbf{x}) - q_i(\mathbf{x}) {}_{x_i}^{\text{RL}} \mathcal{D}_{b_i(\mathbf{x})}^{\beta_i} u(\mathbf{x}) \right) + f(\mathbf{x}, t), & \mathbf{x} \in \Omega, \\ u(\mathbf{x}, 0) = \phi(\mathbf{x}), & \mathbf{x} \in \Omega, \\ u(\mathbf{x}, t) = 0, & (\mathbf{x}, t) \in \Omega^c \times (0, T]. \end{cases} \quad (49)$$

where $p_i(\mathbf{x}) > 0, q_i(\mathbf{x}) > 0$.

For equation (49), the Crank-Nicolson FEM scheme can be written as

$$\begin{cases} (\bar{\partial}_t u_h^j, v) + a(u_h^{j-\frac{1}{2}}, v) = (f^{j-\frac{1}{2}}, v), & \forall v \in V_h, \quad 1 \leq j \leq n_T, \\ u_h^0 = P\phi, \end{cases} \quad (50)$$

where P is a projection operator and

$$a(u, v) = \sum_{i=1}^3 \left((p_i(\mathbf{x}) {}_{a_i(\mathbf{x})}^{\text{RL}} \mathcal{D}_{x_i}^{\beta_i} u, \mathcal{D}_i v) - (q_i(\mathbf{x}) {}_{x_i}^{\text{RL}} \mathcal{D}_{b_i(\mathbf{x})}^{\beta_i} u, \mathcal{D}_i v) \right). \quad (51)$$

In the following, we will give two numerical examples of this problem.

Example 4.3. Assume Ω is unit cubic $(0, 1) \times (0, 1) \times (0, 1)$. Set $p(\mathbf{x}) = (x_1, x_2, x_3)$ and $q(\mathbf{x}) = (1 - x_1, 1 - x_2, 1 - x_3)$. Let the exact solution be

$$u(\mathbf{x}) = 2^{12} e^{5-t} x_1^2 x_2^2 x_3^2 (x_1 - 1)^2 (x_2 - 1)^2 (x_3 - 1)^2. \quad (52)$$

We solve this equation by scheme (50), and present the results in table 15 and fig. 13. In table 15, we notice that the convergence orders of L^2 errors are bigger than 2.

Table 15: L^2 and L^∞ errors and convergence order for equation (46) at $T = 5$.

β	h	$\ u - u_h\ _{L^2}$	order	$\ u - u_h\ _{L^\infty}$	order
(0.6, 0.6, 0.6)	1/8	8.11e-03		7.40e-02	
	1/16	7.31e-04	3.47	1.23e-02	2.59
	1/32	1.44e-04	2.34	1.31e-03	3.23
(0.8, 0.8, 0.8)	1/8	4.56e-02		4.39e-01	
	1/16	8.75e-03	2.38	1.86e-01	1.24
	1/32	1.73e-03	2.34	3.08e-02	2.59

Example 4.4. Assume Ω is $B_r(0) := \{\mathbf{x} \mid |\mathbf{x}| < r\}$. Set $p = (\cos(x_1), \cos(x_2), \cos(x_3))$, $q = (1 - \cos(x_1), 1 - \cos(x_2), 1 - \cos(x_3))$, and let the exact solution be

$$u(\mathbf{x}) = 16e^{5-t} (x_1^2 + x_2^2 + x_3^2 - r^2)^2. \quad (53)$$

where $r = 0.5$.

Solve this equation by scheme (50), and illustrate the results in table 16 and fig. 15. Some meshes used are shown in fig. 14. In this case, the convergence orders of L^2 error approximate to 2, which verifies the convergence of our method again.

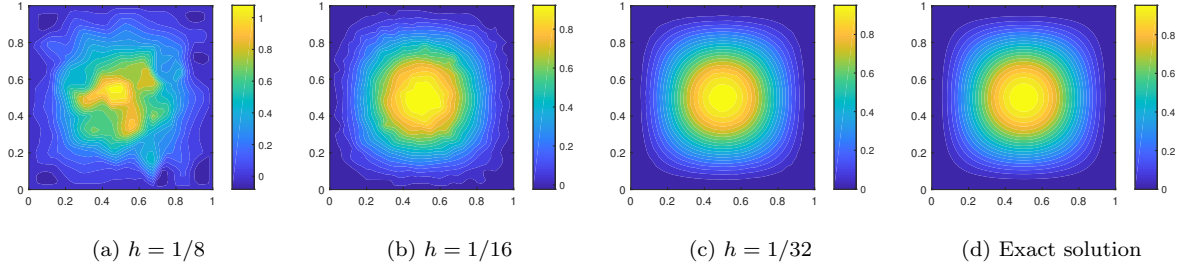


Figure 13: Numerical results and exact results on plane $x_3 = 1/2$ when $\beta = (0.8, 0.8, 0.8)$.

Table 16: L^2 and L^∞ errors and convergence order for equation (46) at $T = 5$.

β	h	$\ u - u_h\ _{L^2}$	order	$\ u - u_h\ _{L^\infty}$	order
(0.75, 0.75, 0.75)	1/8	2.87e-02		3.57e-01	
	1/16	5.74e-03	2.32	7.12e-02	2.33
	1/32	1.49e-03	1.95	2.22e-02	1.68
(0.8, 0.8, 0.8)	1/8	3.96e-02		4.78e-01	
	1/16	8.72e-03	2.18	1.08e-01	2.14
	1/32	2.11e-03	2.05	3.69e-02	1.55
(0.9, 0.9, 0.9)	1/8	6.53e-02		7.43e-01	
	1/16	1.63e-02	2.00	1.96e-01	1.92
	1/32	4.09e-03	1.99	8.42e-02	1.22

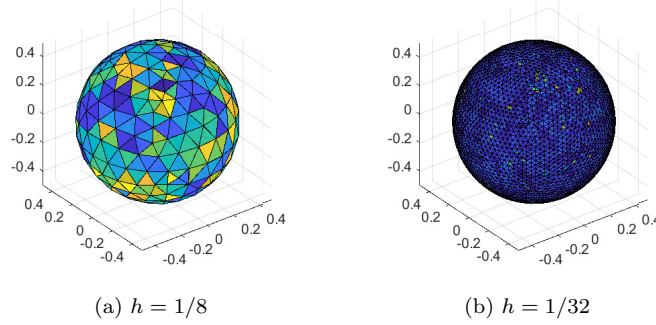


Figure 14: Meshes on a ball with different sizes.

4.2.2. A special case: Riesz spatial fractional reaction-diffusion equations

When set p_i and q_i with suitable values, equation (49) will be an equation with Riesz fractional operators

$$\begin{cases} \frac{\partial u}{\partial t} = \sum_{i=1}^3 {}^{\text{Rz}}\mathcal{D}_{x_i}^{2\alpha_i} u + f(\mathbf{x}, t), & \mathbf{x} \in \Omega, \\ u(\mathbf{x}, 0) = \phi(\mathbf{x}), & \mathbf{x} \in \Omega, \\ u(\mathbf{x}, t) = 0, & (\mathbf{x}, t) \in \Omega^c \times (0, T]. \end{cases} \quad (54)$$

where $1/2 < \alpha_i < 1$ and ${}^{\text{Rz}}\mathcal{D}_{x_i}^{2\alpha_i}$ ($i = 1, 2, 3$) are Riesz fractional derivative operators defined in Section 2.

Denote $V = \cap_{i=1}^3 H_0^{\alpha_i}(\Omega)$, $U = L^2(0, T; V)$. Then the variational problem of equation (54) is Find $u \in U$

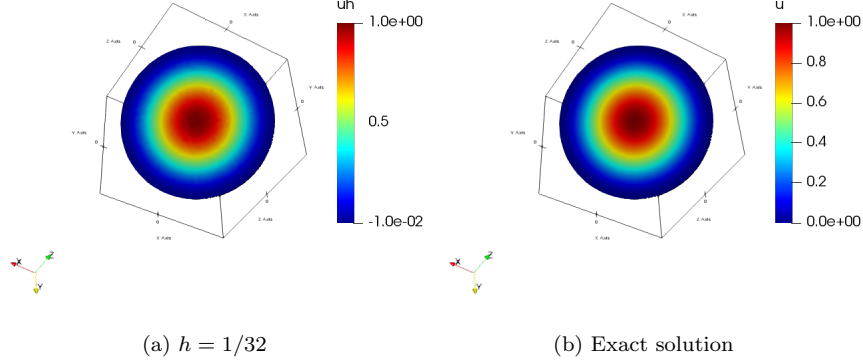


Figure 15: Numerical results of equation (46) and exact solution at $T = 5$.

such that

$$\begin{cases} (u_t, v) + a(u, v) = (f, v), & \forall v \in V \\ u(\mathbf{x}, 0) = \phi(\mathbf{x}), \end{cases} \quad (55)$$

where

$$a(u, v) := \sum_{i=1}^3 c_{\alpha_i} \left((a_i(\mathbf{x}) \mathcal{D}_{x_i}^{\alpha_i} u, x_i \mathcal{D}_{b_i(\mathbf{x})}^{\alpha_i} v) + (x_i \mathcal{D}_{b_i(\mathbf{x})}^{\alpha_i} u, a_i(\mathbf{x}) \mathcal{D}_{x_i}^{\alpha_i} v) \right). \quad (56)$$

Then the Crank-Nicolson FEM scheme can be written as

$$(\bar{\partial}_t u_h^j, v) + a(u_h^{j-\frac{1}{2}}, v) = (f^{j-\frac{1}{2}}, v), \quad \forall v \in V_h, \quad j \geq 1, \quad (57)$$

with $u_h^0 = P\phi$.

By standard analysis process of Crank-Nicolson FEM for parabolic problems[41, Chapter 1], we obtain the following convergence theorem.

Theorem 4.1 (convergence). *Let $\lambda < \mu \leq s + 1$. Suppose that the exact solution $u \in L^\infty(0, T; H_0^\mu(\Omega))$, $u_t \in L^2(0, T; H_0^\mu)$, and $u_{tt} \in L^2(0, T; H^\lambda(\Omega))$. Assume $u_{ttt} \in L^2(0, T; L^2(\Omega))$ and $\phi \in H^\mu(\Omega)$. Then we have*

$$\|u_h(T) - u(T)\|^2 \leq Ch^{2\mu} \left(\|\phi\|_{H^\mu}^2 + \int_0^T \|u_t\|_{H^\mu}^2 ds \right) + C\tau^4 \left(\int_0^T \|u_{ttt}(s)\|^2 ds + \int_0^T \|u_{tt}(s)\|_\alpha^2 ds \right). \quad (58)$$

In the followings, two numerical examples are presented to verify the theoretical result in Theorem 4.1.

Example 4.5. Test the problem on unit cube $\Omega = (0, 1) \times (0, 1) \times (0, 1)$ with solution

$$u(\mathbf{x}, t) = 2^{12} e^{1-t} x_1^2 x_2^2 x_3^2 (x_1 - 1)^2 (x_2 - 1)^2 (x_3 - 1)^2. \quad (59)$$

In this example, choose parameter $T = 1$, solve the problem with different α , and present the results in table 17 and fig. 16. An $O(h^2)$ convergence rate is observed, which agrees well with the theoretical result of Theorem 4.1.

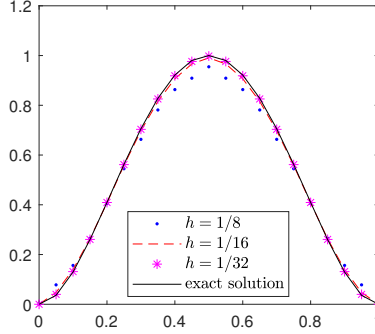
Example 4.6. Consider the problem (54) on unit ball $B_1(0)$ in \mathbb{R}^3 with exact solution

$$u(\mathbf{x}, t) = e^{1-t} (x_1^2 + x_2^2 + x_3^2 - 1)^2. \quad (60)$$

In this example, choose parameters $T = 1$. Firstly, set $\tau = 0.001$ and let $h = \frac{1}{4}, \frac{1}{8}, \frac{1}{16}$. The results at $T = 1$ on different meshes are illustrate in fig. 17. Table 18 shows the spatial convergence orders. The convergence orders of errors in L^2 norm are approximate to 2, which fit well with the result in Theorem 4.1. Now, set $h = \tau$ when $\tau = \frac{1}{4}, \frac{1}{8}, \frac{1}{16}$ and show the results in table 19. From the table we can see the convergence order in temporal direction is also 2.

Table 17: Errors and Convergence order for h with $h = \tau$.

α	h	$\ u - u_h\ _{L^2}$	order	$\ u - u_h\ _{L^\infty}$	order	$ u - u_h _\alpha$	order
(0.8, 0.8, 0.8)	1/8	9.42e-03		4.52e-02		5.90e-02	
	1/16	2.42e-03	1.96	9.23e-03	2.29	1.79e-02	1.72
	1/32	5.85e-04	2.05	2.10e-03	2.14	5.83e-03	1.62
(0.8, 0.85, 0.9)	1/8	1.10e-02		5.45e-02		7.32e-02	
	1/16	3.03e-03	1.86	1.17e-02	2.22	2.41e-02	1.60
	1/32	7.80e-04	1.96	3.57e-03	1.71	1.99e-02	0.28

Figure 16: Numerical results on line $x_2 = 1/2, x_3 = 1/2$ for equation (54) on unit cube.Table 18: Errors and convergence order for $\alpha = (0.9, 0.9, 0.9)$ and $\tau = 0.001$ on unit ball.

h	$\ u - u_h\ _{L^2}$	order	$\ u - u_h\ _{L^\infty}$	order	$ u - u_h _\alpha$	order
1/4	3.39e-02		5.31e-02		1.16e-01	
1/8	8.14e-03	2.06	1.34e-02	1.98	4.10e-02	1.50
1/16	2.20e-03	1.89	3.82e-03	1.81	1.77e-02	1.21

Table 19: Errors and convergence order for different α with $h = \tau$ on unit ball.

α	τ	$\ u - u_h\ _{L^2}$	order	$\ u - u_h\ _{L^\infty}$	order	$ u - u_h _\alpha$	order
(0.9, 0.9, 0.9)	1/4	3.97e-02		6.03e-02		1.30e-01	
	1/8	9.71e-03	2.03	1.42e-02	2.09	4.09e-02	1.67
	1/16	2.61e-03	1.89	4.03e-03	1.81	1.60e-02	1.35
(0.85, 0.9, 0.95)	1/4	4.32e-02		6.51e-02		1.40e-01	
	1/8	1.06e-02	2.03	1.54e-02	2.07	4.44e-02	1.66
	1/16	2.83e-03	1.91	4.22e-03	1.87	1.74e-02	1.35

5. Conclusion

In this paper, we introduced algorithms to assemble fractional stiffness matrix for inner product with fractional derivatives on 3-D domains and the procedure is described in detail. Particularly, we search the integral path by a ray-simplex algorithm which can speedup procedures of assembling fractional stiffness matrices. It is a simple algorithm to compute intersection segments of integral paths with elements and it can be used in any n -dimensional space. Furthermore, we solved 3-D steady/transient fractional problems by the algorithms. Specifically, Crank-Nicolson FEM method is developed to approach the Riesz spatial fractional diffusion equations on convex domain in \mathbb{R}^3 which is seldom solved before. The experiment results show that the method has convergence order $O(h^2 + \tau^2)$, which is consistent with the theoretical results.

Although we present a valid method on searching integral path, the assembly of the fractional stiffness matrix is still much slower than the integer order stiffness matrix. Table 20 shows the comparison of time

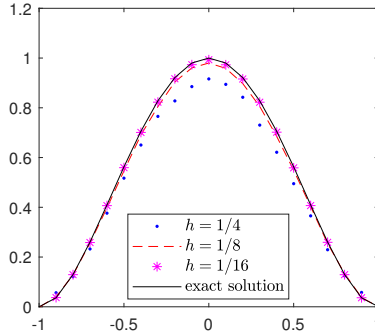


Figure 17: Numerical results on line $x_2 = 0, x_3 = 0$ for equation (54) on unit ball.

Table 20: Comparison of time used in solving fractional and integer elliptic equations

Number of elements	Fractional elliptic equation		Elliptic equation	
	Assemble matrix	Solve linear equations	Assemble matrix	Solve linear equations
4061	35.61s	0.02s	0.92s	0.03s
32683	4m 17.65s	0.18s	4.10s	0.05s
64740	11m 34.60s	0.52s	8.96s	0.09s
126804	29m 55.31s	1.98s	15.83s	0.26s
268418	1h 36m 38.75s	8.62s	33.18s	0.73s

used in solving fractional and integer elliptic equations. Notice that when the Number of elements is 268418, the time cost in assembling fractional stiffness matrix is approximately one and a half hour, while assembly of integer stiffness matrix only used thirty seconds. There is a big gap here. In-depth research is needed on fast algorithms on assembly of fractional stiffness matrix on irregular domains. In the future, we will open source code for everyone to use and improve.

In the numerical experiments, we have noticed that there still is a lot of room to improve the accuracy of inner product of fractional derivatives because of the Gaussian quadrature used in computing inner product. In the future work, we shall work in this regard.

Acknowledgements

This research was supported by the National Natural Science Foundation of China (Grant No.11471262 and No.11601432).

References

References

- [1] Gabriel Acosta, Francisco M. Bersetche, and Juan Pablo Borthagaray. A short FE implementation for a 2d homogeneous dirichlet problem of a fractional laplacian. *Comput. Math. Appl.*, 74(4):784–816, 2017.
- [2] Gabriel Acosta and Juan Pablo Borthagaray. A fractional laplace equation: regularity of solutions and finite element approximations. *SIAM J. Numer. Anal.*, 55(2):472–495, 2017.
- [3] Mark Ainsworth and Christian Glusa. Hybrid finite element–spectral method for the fractional Laplacian: Approximation theory and efficient solver. *SIAM J. Sci. Comput.*, 40(4):A2383–A2405, 2018.
- [4] David A. Benson, Stephen W. Wheatcraft, and Mark M. Meerschaert. Application of a fractional advection-dispersion equation. *Water Resour. Res.*, 36:1403–1412, 2000.

- [5] Juan Pablo Borthagaray, Leandro M. Del Pezzo, and Sandra Martínez. Finite element approximation for the fractional eigenvalue problem. *J. Sci. Comput.*, 77(1):308–329, 2018.
- [6] Weiping Bu, Yifa Tang, Yingchuan Wu, and Jiye Yang. Crank-Nicolson ADI Galerkin finite element method for two-dimensional fractional FitzHugh-Nagumo monodomain model. *Appl. Math. Comput.*, 257:355–364, 2015.
- [7] Weiping Bu, Yifa Tang, Yingchuan Wu, and Jiye Yang. Finite difference/finite element method for two-dimensional space and time fractional Bloch-Torrey equations. *J. Comput. Phys.*, 293:264–279, 2015.
- [8] Weiping Bu, Yifa Tang, and Jiye Yang. Galerkin finite element method for two-dimensional Riesz space fractional diffusion equations. *J. Comput. Phys.*, 276:26–38, 2014.
- [9] Alfonso Bueno-Orovio, David Kay, and Kevin Burrage. Fourier spectral methods for fractional-in-space reaction-diffusion equations. *BIT Numer. Math.*, 54(4):937–954, 2014.
- [10] Luis Caffarelli and Luis Silvestre. An extension problem related to the fractional Laplacian. *Comm. Partial Differential Equations*, 32(8):1245–1260, 2007.
- [11] Cem Çelik and Melda Duman. Finite element method for a symmetric tempered fractional diffusion equation. *Appl. Numer. Math.*, 120:270–286, 2017.
- [12] Mehdi Dehghan and Mostafa Abbaszadeh. An efficient technique based on finite difference/finite element method for solution of two-dimensional space/multi-time fractional Bloch-Torrey equations. *Appl. Numer. Math.*, 131:190–206, 2018.
- [13] Mehdi Dehghan and Mostafa Abbaszadeh. A finite difference/finite element technique with error estimate for space fractional tempered diffusion-wave equation. *Comput. Math. Appl.*, 75(8):2903–2914, 2018.
- [14] Weihua Deng. Finite element method for the space and time fractional Fokker-Planck equation. *SIAM J. Numer. Anal.*, 47(1):204–226, 2008.
- [15] Ning Du and Hong Wang. A fast finite element method for space-fractional dispersion equations on bounded domains in \mathbb{R}^2 . *SIAM J. Sci. Comput.*, 37(3):A1614–A1635, 2015.
- [16] Vincent J. Ervin and John Paul Roop. Variational formulation for the stationary fractional advection dispersion equation. *Numer. Methods Partial Differential Equations*, 22(3):558–576, 2006.
- [17] Vincent J. Ervin and John Paul Roop. Variational solution of fractional advection dispersion equations on bounded domains in \mathbb{R}^d . *Numer. Methods Partial Differential Equations*, 23(2):256–281, 2007.
- [18] Wenping Fan, Xiaoyun Jiang, Fawang Liu, and Vo Anh. The unstructured mesh finite element method for the two-dimensional multi-term time-space fractional diffusion-wave equation on an irregular convex domain. *J. Sci. Comput.*, 77(1):27–52, 2018.
- [19] Wenping Fan, Fawang Liu, Xiaoyun Jiang, and Ian Turner. A novel unstructured mesh finite element method for solving the time-space fractional wave equation on a two-dimensional irregular convex domain. *Fract. Calc. Appl. Anal.*, 20(2), 2017.
- [20] Wenping Fan and Haitao Qi. An efficient finite element method for the two-dimensional nonlinear time-space fractional Schrödinger equation on an irregular convex domain. *Appl. Math. Lett.*, 86:103–110, 2018.
- [21] L. B. Feng, P. Zhuang, F. Liu, I. Turner, and Y. T. Gu. Finite element method for space-time fractional diffusion equation. *Numer. Algorithms*, 72(3):749–767, 2016.
- [22] Andrew Glassner. *An Introduction to Ray Tracing*. Elsevier Science, 1989.

- [23] Rudolf Gorenflo, Francesco Mainardi, Enrico Scalas, and Marco Raberto. Fractional calculus and continuous-time finance III : the diffusion limit. In Michael Kohlmann and Shanjian Tang, editors, *Mathematical Finance*, pages 171–180, Basel, 2001. Birkhäuser Basel.
- [24] Qingguang Guan and Max Gunzburger. θ schemes for finite element discretization of the space-time fractional diffusion equations. *J. Comput. Appl. Math.*, 288:264–273, 2015.
- [25] Bangti Jin, Raytcho Lazarov, Joseph Pasciak, and William Rundell. Variational formulation of problems involving fractional order differential operators. *Math. Comput.*, 84(296):2665–2700, 2015.
- [26] Bangti Jin, Raytcho Lazarov, Joseph Pasciak, and Zhi Zhou. Error analysis of a finite element method for the space-fractional parabolic equation. *SIAM J. Numer. Anal.*, 52(5):2272–2294, 2014.
- [27] Bangti Jin, Raytcho Lazarov, and Zhi Zhou. A Petrov-Galerkin finite element method for fractional convection-diffusion equations. *SIAM J. Numer. Anal.*, 54(1):481–503, 2016.
- [28] Bangti Jin and Zhi Zhou. A finite element method with singularity reconstruction for fractional boundary value problems. *ESAIM Math. Model. Numer. Anal.*, 49(5):1261–1283, 2015.
- [29] Patrick Keast. Moderate-degree tetrahedral quadrature formulas. *Comput. Methods Appl. Mech. Eng.*, 55(3):339–348, 1986.
- [30] Mateusz Kwaśnicki. Ten equivalent definitions of the fractional Laplace operator. *Fract. Calc. Appl. Anal.*, 20(1), 2017.
- [31] Meng Li, Xian-Ming Gu, Chengming Huang, Mingfa Fei, and Guoyu Zhang. A fast linearized conservative finite element method for the strongly coupled nonlinear fractional schrödinger equations. *J. Comput. Phys.*, 358:256–282, 2018.
- [32] Meng Li, Chengming Huang, and Nan Wang. Galerkin finite element method for the nonlinear fractional Ginzburg-Landau equation. *Appl. Numer. Math.*, 118:131–149, 2017.
- [33] Meng Li, Chengming Huang, and Pengde Wang. Galerkin finite element method for nonlinear fractional schrödinger equations. *Numer. Algorithms*, 74(2):499–525, 2016.
- [34] Meng Li, Chengming Huang, and Zongbiao Zhang. Unconditional error analysis of Galerkin FEMs for nonlinear fractional Schrödinger equation. *Appl. Anal.*, 97(2):295–315, 2016.
- [35] Meng Li and Yong-Liang Zhao. A fast energy conserving finite element method for the nonlinear fractional Schrödinger equation with wave operator. *Appl. Math. Comput.*, 338:758–773, 2018.
- [36] Yongshan Li, Huanzhen Chen, and Hong Wang. A mixed-type Galerkin variational formulation and fast algorithms for variable-coefficient fractional diffusion equations. *Math. Methods Appl. Sci.*, 40(14):5018–5034, 2017.
- [37] Lukasz Płociniczak. Analytical studies of a time-fractional porous medium equation. derivation, approximation and applications. *Commun. Nonlinear Sci. Numer. Simul.*, 24(1-3):169–183, 2015.
- [38] John Paul Roop. *Variational solution of the fractional advection dispersion equation*. PhD thesis, Clemson University, 2004.
- [39] John Paul Roop. Computational aspects of FEM approximation of fractional advection dispersion equations on bounded domains in \mathbb{R}^2 . *J. Comput. Appl. Math.*, 193(1):243–268, 2006.
- [40] Enrico Scalas, Rudolf Gorenflo, and Francesco Mainardi. Fractional calculus and continuous-time finance. *Phys. A*, 284(1-4):376–384, 2000.
- [41] Vidar Thomée. *Galerkin Finite Element Methods for Parabolic Problems*. Springer Berlin Heidelberg, 1997.

- [42] Hong Wang and Danping Yang. Wellposedness of variable-coefficient conservative fractional elliptic differential equations. *SIAM J. Numer. Anal.*, 51(2):1088–1107, 2013.
- [43] Hong Wang, Danping Yang, and Shengfeng Zhu. Inhomogeneous Dirichlet boundary-value problems of space-fractional diffusion equations and their finite element approximations. *SIAM J. Numer. Anal.*, 52(3):1292–1310, 2014.
- [44] Hong Wang, Danping Yang, and Shengfeng Zhu. Accuracy of finite element methods for boundary-value problems of steady-state fractional diffusion equations. *J. Sci. Comput.*, 70(1):429–449, 2016.
- [45] Qinwu Xu and Jan S. Hesthaven. Discontinuous Galerkin method for fractional convection-diffusion equations. *SIAM J. Numer. Anal.*, 52(1):405–423, 2014.
- [46] Zongze Yang, Zhanbin Yuan, Yufeng Nie, Jungang Wang, Xiaogang Zhu, and Fawang Liu. Finite element method for nonlinear Riesz space fractional diffusion equations on irregular domains. *J. Comput. Phys.*, 330:863–883, 2017.
- [47] Hongmei Zhang, Fawang Liu, and Vo V. Anh. Galerkin finite element approximation of symmetric space-fractional partial differential equations. *Appl. Math. Comput.*, 217(6):2534–2545, 2010.
- [48] Yiqi Zhang, Xing Liu, Milivoj R. Belić, Weiping Zhong, Yanpeng Zhang, and Min Xiao. Propagation dynamics of a light beam in a fractional schrödinger equation. *Phys. Rev. Lett.*, 115(18), 2015.
- [49] Yong Zhang, David A. Benson, and Donald M. Reeves. Time and space nonlocalities underlying fractional-derivative models: Distinction and literature review of field applications. *Adv. in Water Res.*, 32(4):561–581, April 2009.
- [50] Meng Zhao, Aijie Cheng, and Hong Wang. A preconditioned fast Hermite finite element method for space-fractional diffusion equations. *Discrete and Continuous Dynamical Systems - Series B*, 22(9):3529–3545, 2017.
- [51] Xuan Zhao, Xiaozhe Hu, Wei Cai, and George Em Karniadakis. Adaptive finite element method for fractional differential equations using hierarchical matrices. *Comput. Methods Appl. Mech. Eng.*, 325:56–76, 2017.
- [52] Yanmin Zhao, Weiping Bu, Jianfei Huang, Da-Yan Liu, and Yifa Tang. Finite element method for two-dimensional space-fractional advection-dispersion equations. *Appl. Math. Comput.*, 257:553–565, 2015.
- [53] Zhengang Zhao and Changpin Li. Fractional difference/finite element approximations for the time-space fractional telegraph equation. *Appl. Math. Comput.*, 219(6):2975–2988, 2012.
- [54] Zhengang Zhao and Changpin Li. A numerical approach to the generalized nonlinear fractional Fokker-Planck equation. *Comput. Math. Appl.*, 64(10):3075–3089, 2012.
- [55] Yunying Zheng, Changpin Li, and Zhengang Zhao. A note on the finite element method for the space-fractional advection diffusion equation. *Comput. Math. Appl.*, 59(5):1718–1726, 2010.
- [56] P. Zhuang, F. Liu, I. Turner, and Y.T. Gu. Finite volume and finite element methods for solving a one-dimensional space-fractional Boussinesq equation. *Appl. Math. Model.*, 38(15-16):3860–3870, 2014.